







Highly Biocompatible Lamellar Liquid Crystals Based on Hempseed or Flaxseed Oil with Incorporated Betamethasone Dipropionate: A Bioinspired Multi-Target Dermal Drug Delivery System for Atopic Dermatitis Treatment

Mercedes Vitek ¹, Žiga Medoš ², Zoran Lavrič ¹, Matjaž Jeras ³, Odon Planinšek ¹, Alenka Zvonar Pobirk ¹, Mirjam Gosenca Matjaž ¹

¹Department of Pharmaceutical Technology, Faculty of Pharmacy, University of Ljubljana, Ljubljana, Slovenia; ²Chair of Physical Chemistry, Faculty of Chemistry and Chemical Technology, University of Ljubljana, Ljubljana, Slovenia; ³Department of Clinical Biochemistry, Faculty of Pharmacy, University of Ljubljana, Ljubljana, Slovenia

Correspondence: Alenka Zvonar Pobirk; Mirjam Gosenca Matjaž, Department of Pharmaceutical Technology, Faculty of Pharmacy, University of Ljubljana, Aškerčeva cesta 7, 1000, Ljubljana, Slovenia, Tel +386 147 69 652; +386 147 69 616, Email alenka.zvonar-pobirk@ffa.uni-lj.si; mirjam.gosenca.matjaz@ffa.uni-lj.si

Purpose: Atopic dermatitis (AD) is the most common chronic inflammatory skin disease that severely impairs patient's life quality and represents significant therapeutic challenge due to its pathophysiology arising from skin barrier dysfunction. Topical corticosteroids, the mainstay treatment for mild to moderate AD, are usually formulated into conventional dosage forms that are impeded by low drug permeation, resulting in high doses with consequent adverse effects, and also lack properties that would strengthen the skin barrier. Herein, we aimed to develop biomimetic lamellar lyotropic liquid crystals (LLCs), offering a novel alternative to conventional AD treatment.

Methods: In screening studies, pseudoternary phase diagrams alongside polarized light microscopy (PLM) and viscosity measurements were utilized. Next, the selected LCCs underwent comprehensive characterization via PLM, small-angle X-ray scattering, differential scanning calorimetry, and rheological analysis. Lastly, their performance was evaluated and compared with the commercially available reference medicine in chemical stability study, in vitro permeation testing, in vitro safety assessment using cell proliferation assay, inverted light microscopy, and Raman mapping of keratinocytes, besides gap closure assay performed by live-cell imaging.

Results: Formulation (L/T)Ho30, containing the highest amount of lecithin/Tween 80 mixture (21%) and hempseed oil (28%), demonstrated lamellar microstructure with high skin hydration potential and favourable rheological features for skin administration. Moreover, in comparison with the reference medicine, it stood out by providing suitable chemical BD (betamethasone dipropionate) stability, improved 3-fold BD permeation, and excellent biocompatibility with over 85% cell proliferation at all tested concentrations, ensuring keratinocytes' integrity, as well as promoting skin healing with gap closure observed after 36 hours.

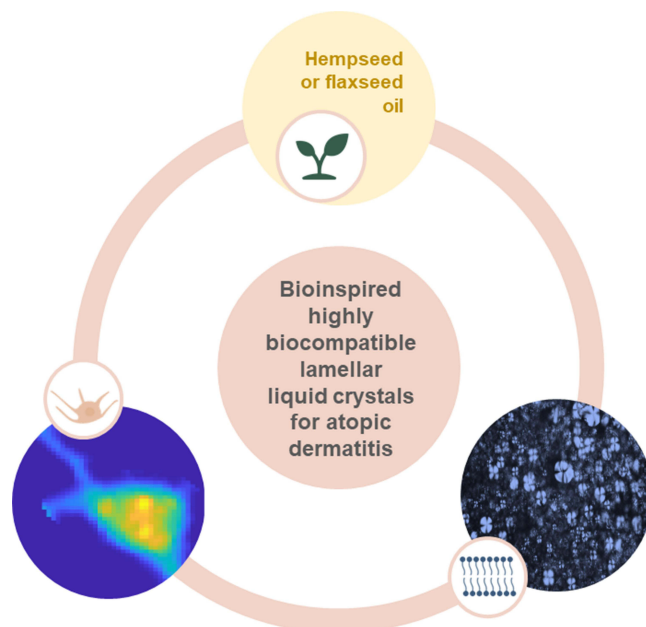
Conclusion: Unique multi-target drug delivery strategy depicted in newly developed bioinspired lamellar LCCs structurally resembling *stratum corneum* intercellular lipids, with incorporated BD drug, and composed of multifunctional components that synergistically strengthen skin barrier, was presented here and shows a promising approach for improved AD treatment.

Keywords: skin barrier, biomimetic, microstructure, keratinocytes, Raman microspectroscopy, gap closure assay

Introduction

Lyotropic liquid crystals (LLCs) are a remarkable class of drug delivery systems that merge the fluid orientation of liquids and the stable orientation order of solids.¹ LLCs are formed by spontaneous self-assembly of amphiphilic

Graphical Abstract



molecules upon contact with an aqueous environment under suitable temperature and concentration conditions. During the formation process, versatile LCC phases (ie, mesophases) can be generated, which are characterized by nanostructured matrices of hydrophilic and hydrophobic domains separated by amphiphilic bilayers. They differ in the orientation arrangement of the molecules and can be classified into hexagonal, cubic, and lamellar mesophases.^{2,3}

Lamellar mesophases represent the forefront LCCs for dermal drug delivery due to their structural similarity to the intercellular lipids of the *stratum corneum*.⁴⁻⁶ More specifically, lamellar LCCs consist of planar bilayers of amphiphilic molecules, in which the polar headgroups face each other while in contact with the aqueous layers, and the nonpolar headgroups are tightly packed together while oriented away from the aqueous molecules.⁷ Owing to their specific microstructure, superior improvements over conventional dermal drug delivery systems have been reported in the scientific literature. Indeed, various studies have shown that lamellar LCCs efficiently solubilize high loadings of hydrophilic, hydrophobic, or amphiphilic drugs,^{8,9} improve their stability,^{10,11} target the site of action, and hence minimize the adverse effects of the incorporated drugs.^{12,13} They are also known for their ability to moisturize the skin for longer period of time^{14,15} and for their excellent viscoelastic properties appropriate for dermal administration.^{16,17}

Considering all the advantages that unambiguously improve patient adherence, lamellar LLCs are particularly suitable for the treatment of chronic skin diseases, which impose a particularly heavy burden on patients and healthcare costs. In this regard, atopic dermatitis (AD) is the most common chronic inflammatory skin disease that severely impairs patients' quality of life. Recent studies have shown that the lifetime prevalence of AD in developed countries is 15–20%.^{18,19} Multiple interrelated genetic, environmental, and immunological factors lead to the development of AD, with the underlying pathophysiology based on skin barrier dysfunction. More specifically, intercellular lipids of the *stratum corneum* are altered in composition and lamellar arrangement,²⁰ transepidermal water loss is increased,²¹ immune responses are triggered,²² and chronic inflammation is present.²³ These pathophysiologic changes subsequently manifest as dry, scaly, and red eczematous lesions with outbreak evolutions accompanied by intense pruritus.¹⁸

Due to its complexity, the disease represents a prominent therapeutic challenge. For mild to moderate AD, which is the most common form of the disease, standard treatment includes regular use of emollients along with intermittent use of topical corticosteroids during the exacerbation phase of AD.²⁴⁻²⁶ Topical corticosteroids are usually formulated into conventional dosage forms such as creams, lotions, and ointments. However, these dosage forms often suffer from low

drug permeation, which commonly results in high doses and the consequent adverse effects. In addition, conventional dosage forms only have the role of carrier systems but do not have skin-supportive properties that would restore the integrity of the atopic skin and contribute to a comprehensive treatment of the disease. Therefore, innovative solutions to these challenges are of high importance.^{27,28}

In the present study, we aimed to develop innovative biomimetic lamellar LCCs as a novel alternative to conventional AD treatment. Following the latest AD treatment guidelines synergistic combination of components with beneficial properties for AD was selected.^{24–26} Hempseed and flaxseed oil, respectively, representing perspective bio-based materials were chosen as the lipid phase of LCCs due to their high content of polyunsaturated essential fatty acids with nourishing, immunoregulatory, and anti-inflammatory effect. In addition, topical application of lipids may repair the deficient lipid composition of atopic skin, resulting in strengthening of the lipid barrier. The oils' unique fatty acids profile also helps to lock in moisture, supporting skin hydration and reducing transepidermal water loss in dry atopic skin.^{29–31} More specifically, hempseed oil contains γ -linolenic acid, which has been shown to regulate immune responses by reducing pro-inflammatory cytokine production, aiding in symptom relief for atopic conditions. In addition, hempseed oil also engages with the skin's endocannabinoid receptors, helping to modulate immune cell activity and maintain immune homeostasis on a cellular level.³² Regarding flaxseed oil, which is especially rich in α -linolenic acid, it may reduce chronic inflammation, helping to prevent and manage flare-ups by modulating immune overactivity.³³ The surfactant phase consisted of biocompatible surfactants, namely lecithin, composed of phospholipids, representing essential components of cell membranes, in combination with Tween 80 or Montanov 68. Notably, lecithin, either alone or in combination with Tween 80 or Montanov 68, has the unique property of forming lamellar mesophases of LCCs.^{34,35} Together with bidistilled water, chosen as the hydrophilic phase, they enable long-lasting skin hydration and thus support skin barrier integrity. Betamethasone dipropionate (BD), a topical corticosteroid, was chosen as an active pharmaceutical ingredient due to its known anti-inflammatory effect on the atopic skin.²⁷ Taken altogether, all of that contributes to a unique multi-target drug delivery strategy for potential AD treatment, which, to the best of our knowledge, has not been described yet.

The development process was systematically divided into three phases. Firstly, in screening studies, pseudoternary phase diagrams were utilized together with polarized light microscopy (PLM) and viscosity measurements for formulation optimization and selection of the most prospective LCCs for further evaluation. Next, the selected LCCs were comprehensively studied using a set of complementary methods, such as PLM, small-angle X-ray scattering (SAXS), differential scanning calorimetry (DSC), and rheological analysis, whereby special attention was given to the aspects that are important for skin administration. Finally, a series of experiments was performed to investigate the performance of the selected LCCs and to compare them with the commercially available reference medicine. The systems were characterized in terms of BD chemical stability as well as BD permeation behavior. Further, their safety was assessed on a human keratinocyte cell line using a well-established cell proliferation assay and inverted light microscopy along with a modern cell biochemical spectral analysis performed by Raman microspectroscopy. Moreover, the potential of the novel LCCs to promote skin healing effect was evaluated by gap closure assay using live-cell imaging.

Materials and Methods

Materials

Lipoid[®] S-100, a soybean lecithin with a phosphatidylcholine content of no less than 94% (m/m), was provided by Lipoid GmbH (Ludwigshafen, Germany). According to the manufacturer's specifications, the fatty acids of the two acyl groups of phosphatidylcholine are palmitic (15%), stearic (3%), oleic and isomers (12%), linoleic (62%), and α -linolenic (5%). Tween[®] 80, polyoxyethylene (20) sorbitan monooleate, with a typical fatty acid composition of approximately 70% oleic acid and other fatty acids such as palmitic acid, was obtained from Sigma-Aldrich (St. Louis, Missouri, USA). Montanov[™] 68, a mixture of cetearyl alcohol and cetearyl glucoside, was obtained from Factory Organica (Ljubljana, Slovenia).

Hempseed oil, with fatty acid composition of palmitic (4–9%), stearic (1–4%), oleic (6–18%), linoleic (46–65%), α -linolenic (14–28%), γ -linolenic (<4%), stearidonic acid (<2%), arachidic (<1.5%) acid, and flaxseed oil, with fatty acid

composition of palmitic (5–8%), stearic (3–8%), oleic (15–39%), linoleic (11–24%), α -linolenic (35–60%), arachidic (<0.5%) acid, were purchased from A.C.E.F. (Fiorenzuola d'Arda, Italy).

BD (98.6% purity) was purchased from Fagron BV (Rotterdam, the Netherlands). Beloderm[®], the commercially available reference medicine containing 0.64 mg/g of BD, was from Belupo (Ljubljana, Slovenia).

Bidistilled water was used for all experiments. All other chemicals and reagents used were of analytical grade.

Pseudoternary Phase Diagram Construction

To determine the concentration range of the components that form LLCs, four pseudoternary phase diagrams were constructed using a water titration method. The surfactant phase consisted of either lecithin/Tween 80 or lecithin/Montanov 68 in a mass ratio of 1/1. Hempseed or flaxseed oil represented the lipid phase. Bidistilled water was used as the hydrophilic phase.

For the titration process, a homogeneous surfactant-lipid mixture with ratios ranging from 90/10 to 10/90% (m/m) was slowly titrated with aliquots of bidistilled water and stirred at room temperature for sufficient time to reach equilibrium. After equilibrium was reached, samples were checked for homogeneity, consistency, and appearance. Homogeneous, viscous, and translucent samples were characterized as LCCs.

Based on the acquired findings, screening studies were then continued for all four combinations of surfactant and lipid phases (ie, all four diagrams: lecithin/Tween 80/hempseed oil/water, lecithin/Tween 80/flaxseed oil/water, lecithin/Montanov 68/hempseed oil/water, and lecithin/Montanov 68/flaxseed oil/water). Specifically, samples from all four diagrams, distributed along a dilution line with a constant surfactant/lipid phase ratio of 60/40 and increasing water content from 10 to 90% (m/m), were selected for further investigation using PLM and rotational tests (ie, viscosity measurements) at 25 °C.

According to the obtained results, eight LCCs were then selected for further evaluation. The exact compositions of the selected unloaded LCCs are presented in Table 1 and the preparation process is described below.

Sample Preparation

LCCs containing Tween 80 were prepared by mixing appropriate amounts of hempseed or flaxseed oil, lecithin, and Tween 80 at 25 °C for sufficient time to form a homogeneous surfactant-lipid mixture. For BD-loaded LCCs containing 0.64 mg/g of BD (ie, dose of the reference medicine), BD was dissolved in the surfactant-lipid mixture. Water was added afterwards during continuous stirring, resulting in the spontaneous formation of LCCs.

LCCs containing Montanov 68 were prepared by mixing appropriate amounts of hempseed or flaxseed oil, lecithin, and Montanov 68 in a water bath set at 50 °C for sufficient time to form a homogeneous surfactant-lipid mixture. In case of BD-loaded LCCs containing 0.64 mg/g of BD (ie, dose of the reference medicine), BD was dissolved in the surfactant-lipid mixture. Water, which was preheated in a water bath set at 50 °C, was added afterwards during continuous stirring, leading to spontaneous formation of LCCs.

Table 1 Composition of the Studied Unloaded LCCs (% M/M); the Letters in the Name of Each System Indicate Lecithin – L, Tween 80 – T, Montanov 68 – M, Hempseed Oil – Ho, Flaxseed Oil – Fo, and the Number Indicates Bidistilled Water Content

	(L/T)Ho30	(L/T)Fo30	(L/T)Ho50	(L/T)Fo50	(L/M)Ho60	(L/M)Fo60	(L/M)Ho80	(L/M)Fo80
Lecithin	21	21	15	15	12	12	6	6
Tween 80	21	21	15	15	–	–	–	–
Montanov 68	–	–	–	–	12	12	6	6
Hempseed oil	28	–	20	–	16	–	8	–
Flaxseed oil	–	28	–	20	–	16	–	8
Bidistilled water	30	30	50	50	60	60	80	80

Polarized Light Microscopy

Microstructural evaluation by polarized light microscopy was employed in screening studies and for unloaded and BD-loaded LCCs. The PLM examination was performed using a CX31-P Upright Microscope (Olympus, Tokyo, Japan). Photomicrographs were obtained at 25 °C, 32 °C, and 37 °C. The magnification was 40 ×.

Small-Angle X-Ray Scattering

Microstructure of unloaded and BD-loaded LCCs was also evaluated by the SAXS method. Measurements were performed with an evacuated Kratky compact camera system (Anton Paar, Graz, Austria) with a block collimating unit, attached to a conventional X-ray generator (Bruker AXS, Karlsruhe, Germany) equipped with a sealed X-ray tube (Cu-anode target type), producing Ni-filtered Cu K α X-rays with a wavelength of 0.154 nm. The tube was operating at 40 kV and 50 mA. The samples were transferred into a standard quartz capillary placed in a thermally controlled sample holder, centered in the X-ray beam. The scattering intensities were measured with a Mythen 1K detector (Dectris, Baden, Switzerland), detecting the scattering pattern within the whole scattering range simultaneously. Measurements were performed at 25 °C, 32 °C, and 37 °C. For each sample and temperature, three SAXS curves were recorded with a sampling time of 1 minute, averaged to ensure reliable statistics and subsequently corrected for solvent scattering. The interlayer spacing d was calculated using Equation 1 where q_1 is the value of the scattering vector at the first peak maximum in the scattering curve.

$$d = 2\pi/q_1 \quad (1)$$

Differential Scanning Calorimetry

DSC characterization was performed for individual components (hempseed oil, flaxseed oil, lecithin, Tween 80, Montanov 68, bidistilled water, and BD), unloaded, and BD-loaded LCCs to analyze the water state within the systems and drug-system intermolecular interactions. A DSC 1 differential scanning calorimeter (Mettler Toledo, Greifensee, Switzerland) was used. Approximately 10 mg of each sample was accurately weighed into a small aluminum pan. An empty pan was used as a reference. Nitrogen was used as a purge gas at a flow rate of 50 mL/min. Two cooling and two heating scans were recorded during each measurement. First, the samples were cooled from 20 °C to –70 °C, kept at –70 °C for 15 minutes, and heated to 40 °C. Afterwards, samples were cooled down to 20 °C again, kept at 20 °C for 15 minutes, and then further cooled to –70 °C, kept at –70 °C for 15 minutes, and heated to 200 °C. All cooling and heating rates were 5 K/min.

Rheological Analysis

Rheology measurements were carried out in screening studies and for unloaded and BD-loaded LCCs. Rotational and oscillatory tests were performed using a Physica MCR 301 rheometer equipped with RheoCompass software (Anton Paar GmbH, Graz, Austria) at 25 ± 0.1 °C, 32 ± 0.1 °C, and 37 ± 0.1 °C. Experiments were performed in duplicate. Rotational tests were carried out to determine the viscosity (η), which was calculated according to the Equation 2 where τ is the shear stress and $\dot{\gamma}$ is the shear rate.

$$\eta = \tau/\dot{\gamma} \quad (2)$$

Oscillatory tests were employed to define the storage (elastic; G') and loss (viscous; G'') moduli, which were calculated using Equations 3 and 4, respectively, where τ is the shear stress, γ is the deformation, and δ is the phase shift angle.

$$G' = (\tau/\gamma) \times \cos\delta \quad (3)$$

$$G'' = (\tau/\gamma) \times \sin\delta \quad (4)$$

In addition, complex viscosity (η^*) was calculated according to Equation 5 where τ is the shear stress, γ is the deformation, and ω is the angular frequency.

$$\eta^* = \tau / (\gamma \times \omega) \quad (5)$$

Rotational tests were carried out using a cone and plate measuring system CP50–2 (cone diameter 49.961 mm, cone angle 2.001 °, sample thickness 0.209 mm). The shear rate ranged from 1 s⁻¹ to 100 s⁻¹. For the oscillatory tests, the stress sweep measurements were carried out at a constant frequency of 10.0 s⁻¹ with the purpose to determine the linear viscoelastic region. Afterwards, the oscillatory shear measurements were performed as a function of frequency (0.1–100 s⁻¹) at a small stress (0.1%) chosen within the linear region to ensure the least disturbance of the microstructure.

Chemical Stability Study

BD-loaded LCCs were subjected to accelerated stability testing. For the purpose of comparison, the reference medicine was also tested under the same conditions. All samples were exposed to elevated temperature (40 ± 2 °C) and high relative humidity (75 ± 5% RH) in an ICH 260L climatic chamber (Memmert, Schwabach, Germany). Samples were prepared and analyzed in triplicate. Assessment was carried out immediately after preparation and subsequently every week within a three-month testing period. The nondegraded BD content was quantified using high-performance liquid chromatography (HPLC) analysis. The results of the chemical stability studies of BD were presented as a percentage of its content relative to the initial content. To evaluate the kinetics of BD degradation, the obtained data were fitted with zero (Equation 6) and first (Equation 7) order kinetic equations where c_t is the concentration at time t , c_0 is the concentration at time zero, and k is the degradation rate constant. The most adequate kinetic model was selected based on the correlation coefficient and applied to determine the degradation rate constant.

$$c_t = c_0 - kt \quad (6)$$

$$\ln c_t = c_0 - kt \quad (7)$$

In vitro Permeation Testing

In vitro permeation studies for BD-loaded LCCs and the reference medicine were conducted using Franz diffusion cells (Verrerie Villeurbannaise, Villeurbanne, France) with a diffusion area of 0.785 cm² and a receptor volume of 8 mL. Strat-M[®] membranes (Merck Millipore, Billerica, MA, USA) were mounted between the donor and receptor compartments. Approximately 400 mg of the sample was accurately weighed directly into the donor compartment. The receptor compartment was filled with a phosphate buffer solution (pH = 7.4) containing 40% (v/v) ethanol, constantly stirred at 400 rpm, and thermostated at 32 ± 1 °C. Studies were performed under sink conditions. At predetermined time points (4, 6, 8, 10, 12, and 24 hours) 800 µL aliquots were withdrawn from the receptor compartment and replaced by an equal volume of fresh preheated receptor medium to keep the volume constant. Experiments were performed in sextuplicate. The BD content in the receiver compartment was determined by HPLC analysis. The cumulative amount of permeated BD (Q_t) was plotted as a function of time and calculated using Equation 8, where c_t is the BD concentration of the receptor medium at each sampling time, V_{rm} is the volume of the receptor medium, c_i is the BD concentration at the previous sampling times, V_i is the sampling volume, and S is the diffusion area.

$$Q_t = \left(c_t \times V_{rm} + \sum_{i=0}^{t-1} c_i \times V_i \right) / S \quad (8)$$

High-Performance Liquid Chromatography Analysis

Instrumentation and Chromatographic Conditions

HPLC measurements were carried out using the Agilent 1100 series HPLC system (Agilent Technologies, Santa Clara, CA, USA). Chromatographic separation was performed using XTerra[®] Shield RP18 Column, 125 Å, 5 µm, 4.6 × 250 mm (Waters Corporation, Milford, MA, USA) at 25 °C. The mobile phase was composed of a mixture of acetonitrile and bidistilled water at a ratio of 60/40 (V/V) and the flow rate was maintained at 1.2 mL/min. The volume of injection was 10 µL. Wavelength of UV detector was set at 254 nm with an analysis run duration of 8 minutes.

Method Validation

The method was validated according to the ICH guidelines Q2(R1) in terms of selectivity, linearity, accuracy, precision, limit of detection (LOD), limit of quantification (LOQ), and sample stability. Method selectivity was confirmed as no interferences were detected in the chromatograms of the used solvents, unloaded LCCs, BD-loaded LCCs, and the reference medicine. The calibration curve was linear over the range of 0.001–0.02 mg/mL with the determined $R^2 = 1.0000$. The obtained results for accuracy ($98.5 \pm 1.8\%$), precision (relative standard deviation = 0.6%), and injection repeatability (0.5%) demonstrated that the method was accurate and precise. The determined LOD and LOQ values were 0.0306 mg/L and 0.0928 mg/L, respectively. Sample stability (within $100 \pm 5\%$) was sufficient after 48 hours of storage at 25 °C.

In vitro Safety Assessment

Cell Culture and Treatment

Human keratinocyte cells (NCTC 2544, ICLC, University of Genoa, Genoa, Italy) were cultured as adherent monolayers at 37 °C in a humidified atmosphere of 5% CO₂. Cells were subcultured using trypsin/EDTA (Promega Corporation, Madison, USA) when they reached 80–90% confluence. They were grown in Eagle's Minimal Essential Medium complemented with 10% (V/V) fetal bovine serum, 1% (V/V) nonessential amino acids, 1% (V/V) penicillin/streptomycin mixture, 1% (V/V) 2 mm L-glutamine, and 1% (V/V) penicillin/streptomycin mixture. Cell culture reagents were from Sigma-Aldrich (St. Louis, Missouri, USA).

Cell Proliferation Assay

The effect of unloaded and BD-loaded LCCs, BD alone, and the reference medicine on keratinocyte proliferation was evaluated using the MTS assay (CellTiter 96[®] Aqueous One Solution Cell Proliferation Assay; Promega, Madison, Wisconsin, USA). The assay is founded on conversion of 3-(4,5-dimethylthiazol-2-yl)-5-(3-carboxymethoxyphenyl)-2-(4-sulfophenyl)-2H-tetrazolium, an inner salt, into the soluble formazan product by mitochondrial dehydrogenase enzymes in metabolically active cells. The assessment was performed according to the manufacturer's instructions. Keratinocytes were seeded at a density of 0.5×10^4 cells per well in 96-well plates and incubated in the supplemented medium for 24 hours to adhere. The cells were then treated with samples diluted with the cell medium. The final concentrations to which the cells were exposed were as follows: 0.5, 2.5, 5.0, and 10.0 mg/mL. The cell proliferation was assessed 24 hours after the addition of the samples. The untreated cells were used as a positive control. The absorbance of formazan was read at 490 nm using a Safire2 microplate reader (Tecan Group AG, Männedorf, Switzerland). Experiments were performed in sextuplicate. The results were expressed as the absorbance ratio of treated to untreated control cells, and the percentage of cell proliferation was calculated according to Equation 9 where A_s is the absorbance of the treated cells (sample), A_c the absorbance of the untreated cells (positive control), A_{s0} the absorbance of the sample in cell-free medium, and A_{c0} the absorbance of the medium alone.

$$\% \text{ of cell proliferation} = ((A_s - A_{s0}) / (A_c - A_{c0})) \times 100 \quad (9)$$

Inverted Phase-Contrast Microscopy

Keratinocytes (NCTC 2544) at a density of 2×10^5 cells per well were seeded in 6-well plates with inserted dry-heat sterilized glass coverslip and incubated in the supplemented medium overnight to adhere. The cells were then treated with test solution or supplemented medium (positive control). The final concentration to which the cells were exposed was 5.0 mg/mL. Following a 24-hour incubation, the medium was removed, and a fixation protocol was performed. The cells were fixed with ice-cold 96% ethanol (Kefo, Ljubljana, Slovenia) for 2.5 minutes. Immediately afterwards the cells were washed twice in phosphate buffer solution (pH = 7.4), once in bidistilled water, and then air dried. The morphology of the keratinocytes was visualized and examined using an inverted phase-contrast light microscope (Olympus CKX41, Tokyo, Japan). Photomicrographs were taken at $20 \times$ magnification.

Raman Microspectroscopy

For Raman mapping of cells, keratinocytes (NCTC 2544) were treated with test solution at the same concentration or supplemented medium (positive control) and prepared according to the same fixation protocol as for inverted phase-contrast microscopy. A confocal microscope Xplora Plus (Horiba Instruments, Kyoto, Japan, equipped with a 100 × magnification objective (Olympus MPLFLN100XBDP), was used. Sample step size in XY plane during mapping was set to 1 μm. Laser 532 nm (Nd:YAG) was used as a light source. Raman scattered light from sample was guided through a confocal pinhole set to 500 μm. Grating with 1200 grooves per mm was used to separate the polychromatic Raman signal into constituent wavelengths before entering the detector through a 200 μm wide slit to illuminate a charge coupled device detector (Syncerity, Horiba) cooled to −60 °C. Signal integration time for each point measurement was set to 16 seconds. Each point of the hyperspectral map was an average spectrum made of three consecutive spectral measurements of the same spatial point.

Solo + Mia (Eigenvector Research Inc.) was used for subsequent analysis. Hyperspectral maps were first smoothed with Savitzky-Golay filter (0 order and width of 15 points) and baseline corrected with automated weighted least squares (2nd order). Multivariate curve resolution decomposition procedure with 2 components was then applied to hyperspectral maps. Primary components analysis (with 2 components) was also applied to baseline corrected data to discard background points and points pertaining to specs of dust. From PCA score plots (1st vs 2nd) all the spectra from points pertaining to cells were then manually selected and averaged to make cell averaged spectra.

Gap Closure Assay

The gap closure assay was carried out to investigate the keratinocyte (NCTC 2544) migration in vitro. For this purpose, the CytoSMART Lux2 (Axion Biosystems, Atlanta, Georgia, USA), enabling visualization of the gap closure process over time, was used. The test was performed in a 2-well silicone cell culture insert system enabling the creation of a defined 500 ± 100 μm cell-free gap, pre-inserted into a μ-Dish35 mm, high (ibidi GmbH, Gräfelfing, Germany). Keratinocytes were seeded at a density of 1.61 × 10⁵ cells in 70 μL per each well and incubated in the supplemented medium overnight to adhere. The composition of the supplemented medium: Dulbecco's Modified Eagle Medium with low glucose (1g/L) (Capricorn Scientific GmbH, Germany), stable glutamine, and sodium pyruvate (Capricorn Scientific GmbH, Germany), supplemented with 10% fetal bovine serum (Capricorn Scientific GmbH, Germany) and 1 × antibiotic antimycotic solution (Sigma-Aldrich Chemie GmbH, Germany). After adhesion was reached, the insert was carefully removed, and 2 mL of either test solution or supplemented medium (positive control) were added per μ-Dish. The final concentration to which the cells were exposed was 0.5 mg/mL. The gap closure tests were conducted under standard cell culture conditions in an incubator (37 °C with a humidified atmosphere of 5% CO₂ in air). Gap closure, ie, cell migration was monitored over 48 hours using time-lapse microscopy, with snapshots taken every 30 minutes.

Data and Statistical Analysis

Data and statistical analyses were performed using GraphPad Prism 10.2.0. Unless stated otherwise, all results are expressed as mean ± standard deviation (SD). Multiple comparisons of means (one-way ANOVA, post-hoc Dunnett's multiple comparisons test) were used to substantiate the statistical differences between the compared groups, with a statistically significant value set at $p < 0.05$.

Results and Discussion

Screening Studies for the LCCs Selection

Four pseudoternary phase diagrams were constructed to determine the LCCs formation regions of the lecithin/Tween 80/hempseed oil/water (Figure 1A), lecithin/Tween 80/flaxseed oil/water (Figure 1B), lecithin/Montanov 68/hempseed oil/water (Figure 1C), and lecithin/Montanov 68/flaxseed oil/water (Figure 1D) systems. The ternary phase behavior of the systems was initially analyzed macroscopically. Homogenous, translucent, and semisolid (ie, gel-like) systems were identified as liquid crystalline phases. Because only LCCs were of our interest, no attempt was made to identify in detail other regions of the diagrams where the formation of nonhomogeneous systems, coarse emulsions, or microemulsions

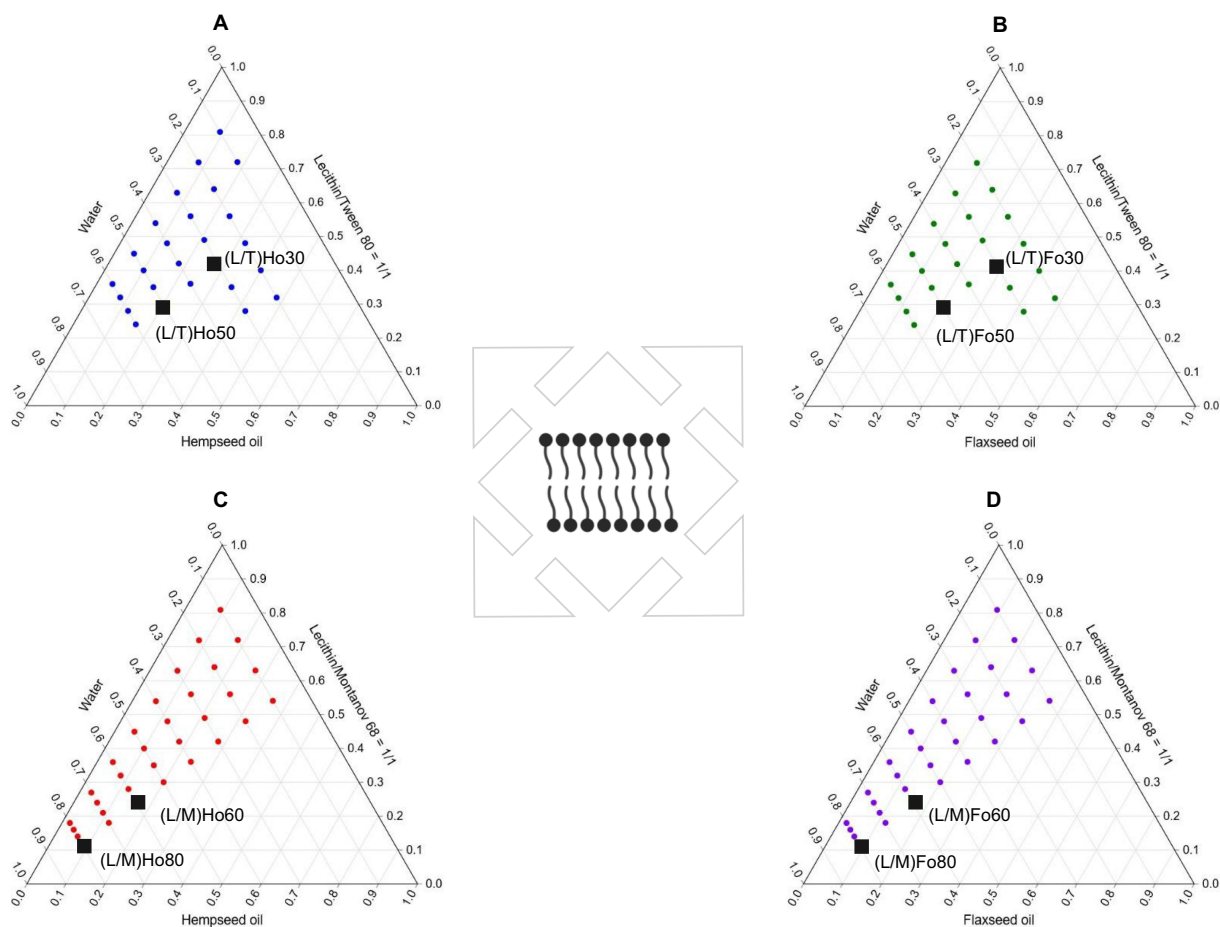


Figure 1 Pseudoternary phase diagrams of the systems composed of **(A)** lecithin/Tween 80/hempseed oil/water, **(B)** lecithin/Tween 80/flaxseed oil/water, **(C)** lecithin/Montanov 68/hempseed oil/water, and **(D)** lecithin/Montanov 68/flaxseed oil/water. The circles show the areas where lamellar LCCs are present, as determined by macroscopic analysis. The selected studied LCCs are marked with a square. A schematic illustration of lamellar LCCs is presented in the middle.

was observed. Coarse emulsions are typically fluid-like and exhibit a milky white appearance. Microemulsions being liquid low-viscous dispersions are, on the other hand, optically transparent systems formed spontaneously. Spontaneous formation is also a characteristic of LCCs, but they are distinguished by their high viscosity or semisolid nature, appearing with a translucent color. A pseudoternary phase diagram study indicated that the type of surfactant had a particularly great impact on the formation of LCCs, while the type of polyunsaturated fatty acids rich lipid did not show any significant effect. Systems containing Tween 80 yielded a wide region of liquid crystalline phases. More precisely, in the first diagram, the range of concentrations at which LCCs were formed was 24–81% for lecithin/Tween 80, 4–48% for hempseed oil, and 10–60% for water. In the second diagram, the concentrations of lecithin/Tween 80, flaxseed oil, and water at which LCCs were formed were 24–72%, 4–48%, and 20–60%, respectively. In contrast, for systems containing Montanov 68, the region of LCCs formation increased considerably with increasing water concentration but also decreased moderately with decreasing surfactant phase content. Therefore, the regions of the liquid crystalline phases obtained were narrower in the case of Montanov 68. The third and fourth diagrams showed that LCCs were formed in regions where the concentrations of lecithin/Montanov 68, hempseed or flaxseed oil, and water were 12–81%, 2–36%, and 10–80%, respectively.

Because LCCs were formed in all four constructed pseudoternary phase diagrams, screening studies continued with the selection of a dilution line for all four combinations of surfactant and lipid phases. Suitable macroscopic properties (ie, consistency and spreadability) of the systems were one of the pivotal selection criteria. In addition, according to the

results of the pseudoternary phase diagram study, LCCs were mainly formed at higher proportions of the surfactant phase, which could potentially cause skin irritation. In view of this, we also considered that the selected systems contained the lowest possible content of the surfactant phase at which LCCs were still formed in all four diagrams. Taken together, systems from all four diagrams distributed along a dilution line with a constant surfactant/lipid phase ratio of 60/40 and increasing water content from 10 to 90% (m/m) were selected for further screening using PLM and rotational tests (ie, viscosity measurements) at 25 °C.

Lamellar LCCs are particularly suitable for skin administration due to their special *stratum corneum*-like structure. Under polarized light microscope, LCCs exhibit characteristic structures for each mesophase, with lamellar mesophases being recognized by the appearance of Maltese crosses.³⁶ PLM analysis revealed that systems containing lecithin/Tween 80 exhibited lamellar mesophases at a water content of 50% (m/m) or less for both oils. In contrast, for systems containing lecithin/Montanov 68, the presence of Maltese cross shapes was confirmed at water contents of 60% (m/m) or higher for both oils. Along with the identification of systems with lamellar mesophases, viscosity measurements were performed to reveal the composition of systems exhibiting optimal viscosities for dermal administration. We found that the viscosities of all analyzed systems were inversely proportional to the water content. Considering all the data from the screening studies, eight LCCs (their composition is reported in Table 1 and highlighted in Figure 1) with lamellar microstructure and favorable rheological characteristics were selected as the most prospective dermal drug delivery systems and enrolled into further characterization studies.

Characterization Studies of the Selected LCCs

Polarized Light Microscopy

PLM is one of the most widely used methods for distinguishing the microstructural variance of different LCCs. Anisotropic LCCs such as lamellar mesophases show characteristic Maltese crosses under polarized light.³⁶ Our photomicrographs (Figure 2) attest their presence in unloaded and BD-loaded LCCs at skin surface temperature (32 °C). Comparable results were also obtained for unloaded and BD-loaded LCCs at room temperature (25 °C) and body temperature (37 °C). The fact that the microstructure is preserved over the entire explored temperature range is important in terms of the administration and storage conditions of these systems.¹⁰ However, besides Maltese crosses, certain additional features were also present in some of the studied LCCs, depending on the surfactant type.

The self-assembly of amphiphiles in an aqueous environment is driven by a balance between the hydrophobic interactions of the nonpolar tails and geometric packing constraints of the polar headgroups. In this regard, the critical packing parameter (CPP) model can be applied to evaluate the self-assembly tendency of amphiphiles and predict the shape of the aggregated structure, respectively. CPP is a geometric expression representing the ratio between the hydrophobic tail volume (v) and the product of the polar headgroup area (a) and the hydrophobic tail length (l). As a guideline, amphiphiles with a CPP below 1 self-assemble into spherical micelles, between 1/3 and 1/2 into cylindrical micelles, and between 1/2 and 1 into vesicles and flexible bilayers. Amphiphiles with a CPP above 1 promote the formation of inverted structures. Planar bilayers, ie, lamellar mesophases, are formed by amphiphiles with a CPP of around 1.³⁷

Our PLM results were consistent with the geometries of the amphiphilic molecules present in the studied systems. Unloaded and BD-loaded LCCs containing lecithin/Tween 80 (ie, (L/T)Ho30, (L/T)Fo30, (L/T)Ho50, and (L/T)Fo50) exhibited numerous Maltese crosses, indicating the predominant existence of lamellar mesophases mimicking *stratum corneum*-like structure. The lamellar phase behavior is related to lecithin, namely to phosphatidylcholine as its principal ingredient because the cross-sectional area of the two hydrocarbon tails is similar to that occupied by the polar head. Accordingly, its CPP value is ~ 1 ,³⁸ which meets the criteria for bilayer formation. In contrast, Tween 80 has only one hydrocarbon tail and a large polar head, which gives it a conical structure with a CPP value of ~ 0.07 ,³⁹ indicating the ability to adopt a high curvature. Nevertheless, only lamellar mesophases were observed in the LCCs containing lecithin/Tween 80. Similar phase behavior of lecithin and Tween 80 has already been reported in the pioneering work of Rong et al⁴⁰ and in more recent research by our group³⁵ and others⁴¹ as well. Apparently, the hydrocarbon tails of both

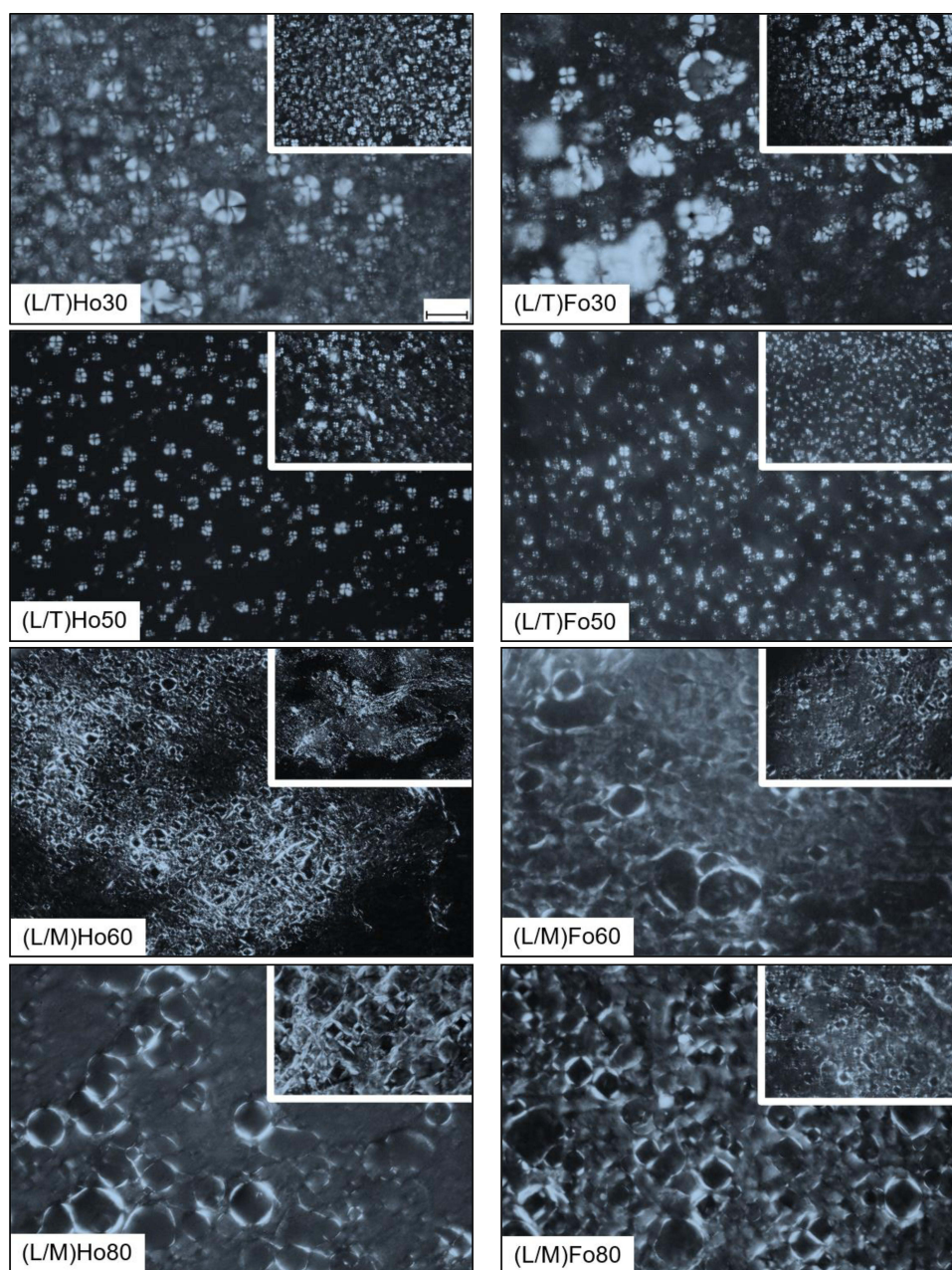


Figure 2 PLM photomicrographs of unloaded (larger photomicrographs) and BD-loaded LCCs (smaller photomicrographs) at 32 °C. The magnification used was 40 ×. The scale bar represents 50 μm.

amphiphiles are packed closely together, whereby lecithin provides a rigid planar arrangement, and Tween 80 contributes to bilayer fluidity.

In contrast, in unloaded and BD-loaded LCCs containing lecithin/Montanov 68 (ie, (L/M)Ho60, (L/M)Fo60, (L/M)Ho80, and (L/M)Fo80) the presence of anisotropic droplets, ie, “onion droplets”, uniformly dispersed into the continuous phase with individual Maltese crosses, was observed. Such photomicrographs indicate a less pronounced lamellar microstructure, which is consistent with literature data⁴² suggesting that both oil droplets and lamellar mesophases are present in such systems. Accordingly, oil droplets act as nuclei for the multilayers of the lamellar LCCs. The driving force for the formation of lamellar mesophases can be attributed to lecithin, which self-assembles into planar bilayers. On the other hand, one of the main constituents of Montanov 68, cetearyl alcohol with a CPP value of ~0.8,⁴³ provides flexibility to the bilayers and promotes the formation of vesicles with entrapped oil droplets.

Small-Angle X-Ray Scattering

The results of the PLM study were further upgraded by the SAXS analysis, which provided a nanoscale understanding of the studied LCCs. Figure 3 shows a scaled plot of the SAXS profiles (scattering intensity I versus scattering vector q) for unloaded and BD-loaded LCCs at 32 °C (skin surface temperature), with the most prominent differences observed among the LCCs with different surfactant types and water contents. SAXS analysis was also performed at 25 °C (room temperature) and 37 °C (body temperature) for unloaded and BD-loaded LCCs, and the obtained results were practically identical to those at 32 °C. Thus, it can be confirmed that the microstructure is preserved at various temperatures important for dermal drug delivery.

X-rays scattered at small angles can result in characteristic peaks known as Bragg peaks. Their position, ie, the scattering vector, can be correlated to the interplanar distances in the sample and thus enables structural characterization through the number and ratio of correlation distances between the obtained peaks. For unloaded and BD-loaded (L/T) Ho30 and (L/T)Fo30, three Bragg peaks were observed at a ratio of 1:2:3, whereas for unloaded and BD-loaded (L/T) Ho50 and (L/T)Fo50, two scattering peaks were observed at a ratio of 1:2. Both patterns are typical of lamellar LCCs. Additional confirmation of the presence of lamellar mesophases was provided by the strong intensities of the scattering peaks.^{9,44} Furthermore, the results of the SAXS measurements carried out on unloaded and BD-loaded (L/M)Ho60 and (L/M)Fo60 showed three broad Bragg peaks at a ratio of 1:2:3, whereas for unloaded and BD-loaded (L/M)Ho80 and (L/M)Fo80, four broad scattering peaks appeared at a ratio of 1:2:3:6. The emergence of broad scattering peaks in such ratios indicates the presence of lamellar mesophases with a low number of stacked bilayers.⁴⁵ Notably, the extinction of

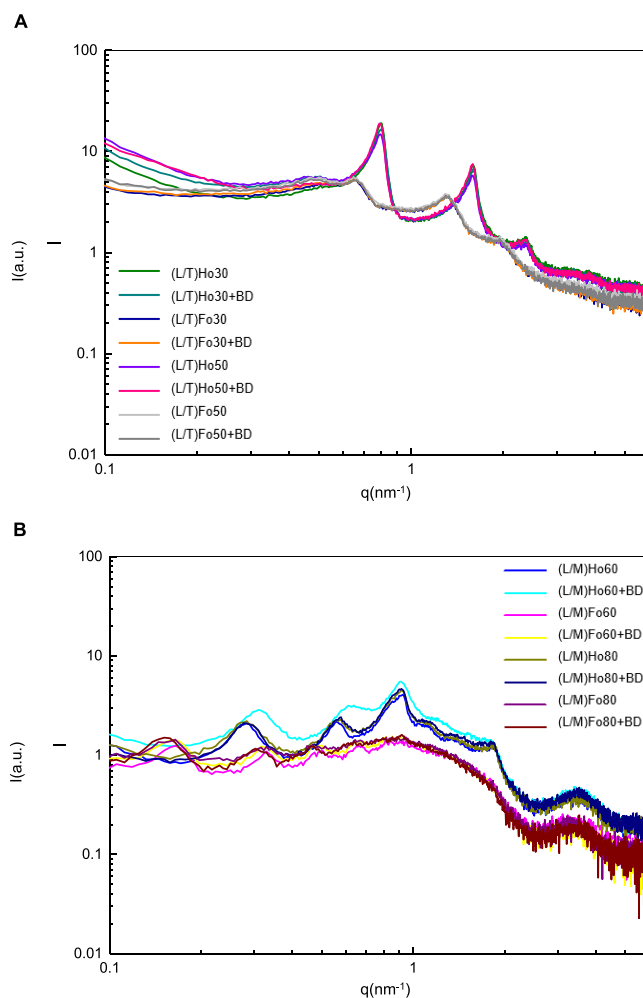


Figure 3 Scattering curves of unloaded and BD-loaded LCCs containing (A) lecithin/Tween 80 and (B) lecithin/Montanov 68 at 32 °C.

the fourth- and fifth-order peaks was also observed for the latter LCCs, suggesting an even larger domain spacing and greater separation distance between the lamellae in these LCCs, respectively.⁴⁶

To further elucidate the distribution and packaging of lamellae in all the studied LCCs, the interlayer spacing d , which represents the distance between the centers of the neighboring surfactant bilayers, was calculated. The corresponding results in Table 2 are in good agreement with the data presented thus far. Namely, the interlayer spacing was found to be a function of surfactant type and water content. It ranged from 7.9 ± 0.1 nm for unloaded and BD-loaded (L/T)Ho30 and (L/T)Fo30 to 39 ± 2 nm for unloaded and BD-loaded (L/M)Ho80 and (L/M)Fo80. The effect of the surfactant type on the interlayer spacing is related to its impact on the formation of different structures (ie, lamellar mesophases, oil droplets) in LCCs. In agreement with the typical “lamellar” swelling law,⁴⁷ these results also indicate that the d -spacing was positively correlated with the water content of the studied LCCs. This phenomenon can be attributed to the increase in the amount of water incorporated into the interlamellar region. Finally, it is important to note that the drug-loaded counterparts exhibited comparable interlayer distances, indicating no or minimal structural rearrangements after BD incorporation into the studied LCCs mimicking *stratum corneum*-like lamellar structure.

Differential Scanning Calorimetry

DSC analysis was performed to evaluate the state of water in unloaded and BD-loaded LCCs, indicating the strength of the interactions between the surfactant molecules and water. In addition, drug–liquid crystalline system interactions were elucidated. DSC analysis included the assessment of individual components and of unloaded and BD-loaded LCCs. The water state differentiation between the studied LCCs was assessed based on the crystallization (T_c) and melting (T_m) temperatures plus the enthalpy of crystallization (ΔH_c) and melting (ΔH_m) obtained by integrating the area of the relevant DSC peaks. For easier interpretation of the obtained results, the DSC thermograms were divided into the dynamic parts of the temperature program. Thus, we obtained the crystallization curves of the first and second cooling cycles plus melting curves of the first and second heating cycles.

On the crystallization curves of the first cooling cycle of individual components (Figure 4A), the crystallization of supercooled bidistilled water was most clearly observed ($T_c = -17.4$ °C; $\Delta H_c = 255.5$ J/g), while no significant thermal events were observed for the other compounds. Further, the crystallization curves and the corresponding data (Table 3) of the first cooling cycle for unloaded (Figure 4B) and BD-loaded (Figure 4C) LCCs clearly show that the crystallization temperatures and areas of the peaks depend on the surfactant type and water content of the system. It is well known that water molecules that interact strongly with the polar headgroups of surfactant molecules cannot form hydrogen bonds with neighboring water molecules. Therefore, they solidify at lower temperatures than those with weaker interactions, and their enthalpy of freezing is lower, in some cases, below the limit of detection. Based on this phenomenon, water can be classified as nonfreezable, freezable interlamellar bound water, or freezable bulk water.⁴⁸

With regard to the unloaded LCCs, on the one hand, the presence of freezable interlamellar bound water was most evidently seen in (L/T)Ho30, (L/T)Fo30, (L/T)Ho50, and (L/T)Fo50. Interestingly, the water crystallization peaks of (L/T)Ho30 and (L/T)Fo30, detected over a wide T_c range and with relatively low ΔH_c suggest the presence of ice in multiple

Table 2 Interlayer Spacing d (Mean \pm SD ($n = 3$)) of Unloaded and BD-Loaded LCCs Determined at 32 °C

	d_1 (nm)		d_2 (nm)		d_3 (nm)		d_4 (nm)	
	Unloaded	BD-Loaded	Unloaded	BD-Loaded	Unloaded	BD-Loaded	Unloaded	BD-Loaded
(L/T)Ho30	7.9 ± 0.1	7.9 ± 0.1	4.0 ± 0.1	4.0 ± 0.1	2.6 ± 0.1	2.6 ± 0.1	-	-
(L/T)Fo30	7.9 ± 0.1	7.9 ± 0.1	4.0 ± 0.1	4.0 ± 0.1	2.6 ± 0.1	2.6 ± 0.1	-	-
(L/T)Ho50	9.7 ± 0.2	9.7 ± 0.2	4.8 ± 0.1	4.8 ± 0.1	-	-	-	-
(L/T)Fo50	9.7 ± 0.2	9.7 ± 0.2	4.8 ± 0.1	4.8 ± 0.1	-	-	-	-
(L/M)Ho60	-	-	20.3 ± 0.7	22.4 ± 0.8	10.1 ± 0.2	11.2 ± 0.2	6.9 ± 0.1	6.9 ± 0.1
(L/M)Fo60	-	-	22.4 ± 0.8	22.4 ± 0.8	11.2 ± 0.2	11.2 ± 0.2	6.9 ± 0.1	6.9 ± 0.1
(L/M)Ho80	39.0 ± 2.0	39.0 ± 2.0	19.0 ± 0.6	19.0 ± 0.6	12.8 ± 0.3	12.8 ± 0.3	7.4 ± 0.4	7.4 ± 0.4
(L/M)Fo80	42.0 ± 3.0	39.0 ± 2.0	20.9 ± 0.6	20.9 ± 0.6	13.4 ± 0.3	12.8 ± 0.3	7.4 ± 0.1	7.4 ± 0.4

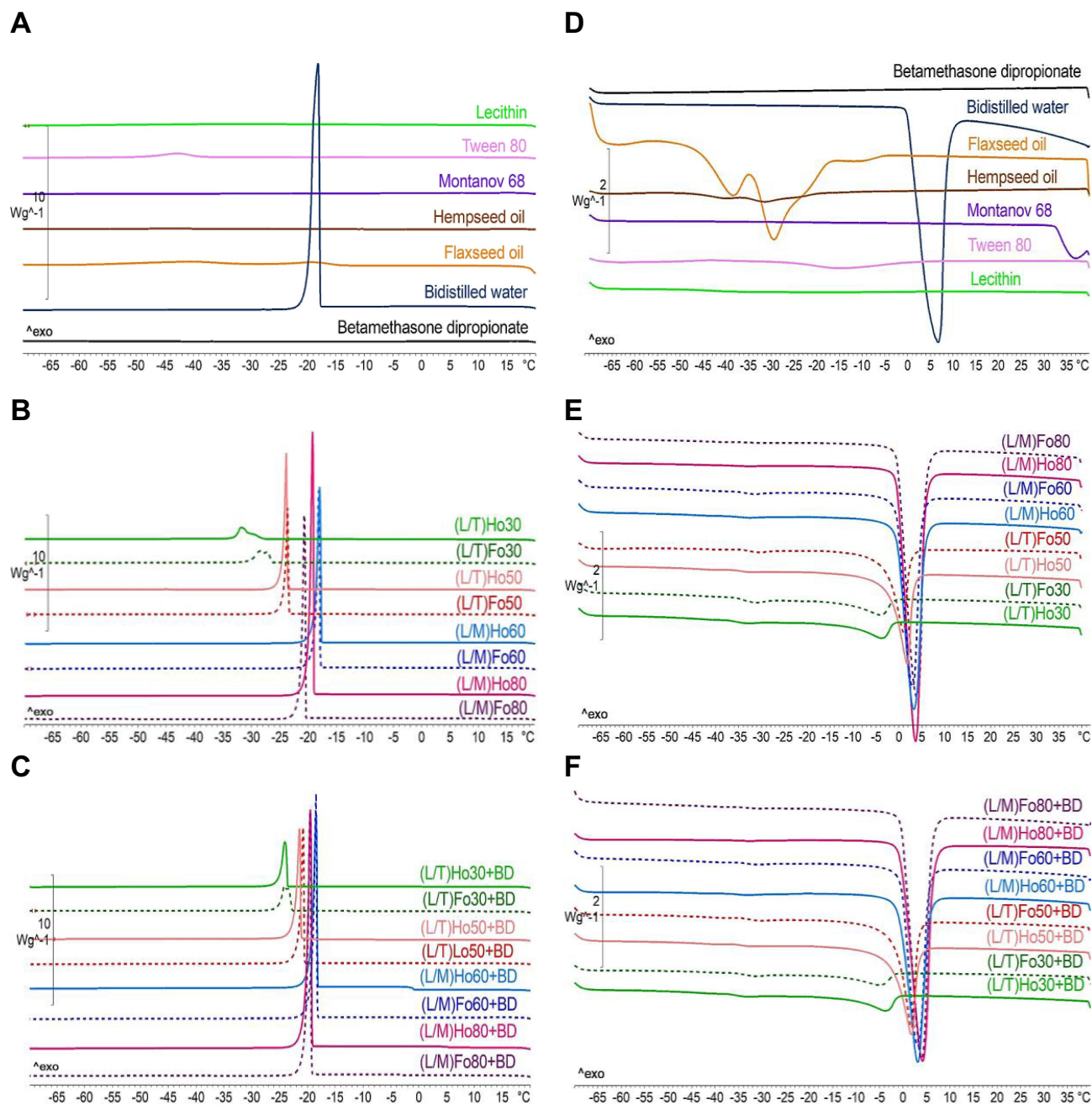


Figure 4 DSC crystallization curves of the first cooling cycle (left side) belonging to (A) individual components, (B) unloaded, (C) and BD-loaded LCCs plus DSC melting curves of the first melting cycle (right side) belonging to (D) individual components, (E) unloaded, (F) and BD-loaded LCCs.

structures.⁴⁹ On the other hand, the predominant existence of freezable bulk water was observed in (L/M)Ho60, (L/M)Fo60, (L/M)Ho80, and (L/M)Fo80, as their T_c and ΔH_c were very similar to that of pure bidistilled water. These results indicate a distinctive lamellar arrangement of the studied LCCs, which corresponds well with the SAXS results. Regarding BD-loaded systems, for the (L/T)Ho30, (L/T)Fo30, (L/T)Ho50 and (L/T)Fo50 the water crystallization peak slightly moved toward higher temperatures and the corresponding enthalpy increased after the drug incorporation. This can be attributed to the lipophilic character of BD and its partitioning into the nonpolar bilayers of these LCCs, with the predominant presence of lamellar mesophases; hence, the interactions between the surfactant and water molecules are weaker than those of the unloaded LCCs. In contrast, in the case of (L/M)Ho60, (L/M)Fo60, (L/M)Ho80, and (L/M)Fo80, there were no noticeable changes in the DSC curves after drug incorporation because BD is most likely

Table 3 DSC Thermodynamic Parameters (ie, Crystallization Temperature and Crystallization Enthalpy) of the First Cooling Cycle of Unloaded and BD-Loaded LCCs

	T_c (°C)		ΔH_c (J/g)	
	Unloaded	BD-Loaded	Unloaded	BD-Loaded
(L/T)Ho30	-29.6	-23.4	31.3	46.9
(L/T)Fo30	-26.2	-22.7	33.4	41.1
(L/T)Ho50	-17.8	-20.8	93.2	89.5
(L/T)Fo50	-17.2	-20.3	135.4	94.1
(L/M)Ho60	-17.5	-17.9	135.1	144.7
(L/M)Fo60	-17.2	-17.6	219.4	151.1
(L/M)Ho80	-18.7	-18.4	193.8	190.3
(L/M)Fo80	-20.4	-18.4	148.6	182.6

incorporated into the oil droplets of these LCCs and thus does not affect the interactions between the surfactant and water molecules. These results strengthen the observations from the PLM photomicrographs, indicating the presence of anisotropic droplets uniformly dispersed in the continuous phase of lamellar LCCs.

Similar conclusions were drawn upon examining the crystallization curves of the second cooling cycle. As for individual components ([Supplementary Figure S1A](#)), only the peak corresponding to the crystallization of supercooled bidistilled water ($T_c = -22.1$ °C; $\Delta H_c = 240.4$ J/g) was again detected here. For unloaded ([Supplementary Figure S1B](#)) and BD-loaded ([Supplementary Figure S1C](#)) LLCs, the crystallization curves were practically identical to those obtained in the first cooling cycle. This allows us to presume that the microstructure of the studied LCCs is thermally stable over a wide temperature range, including the temperature of application and storage of these systems, which again supports the results of the PLM and SAXS studies.

Several thermal events were observed in the melting curves of the first heating cycle for the individual components ([Figure 4D](#)). For interpretation of the results, however, the endothermic peak ($T_m = -0.1$ °C; $\Delta H_m = -282.3$ J/g), which belongs to the melting of bidistilled water ice, should be highlighted here. Further, the melting curves and corresponding data ([Table 4](#)) of the first heating cycle for unloaded ([Figure 4E](#)) and BD-loaded ([Figure 4F](#)) LCCs are in good agreement with the conclusions based on the cooling part of the DSC curves. The positions and areas of the peaks corresponded to the surfactant type and water content of the LCCs. The endothermic peaks belonging to (L/T)Ho30, (L/T)Fo30, (L/T)Ho50, and (L/T)Fo50 reflect the melting of freezable interlamellar water. To note, two broad peaks with low ΔH_m positioned before the peak of pure bidistilled water were observed for (L/T)Ho30 and (L/T)Fo30, confirming that freezable interlamellar water of these LCCs is present in two populations with different bonding mode.⁵⁰ On the contrary, only a sharp peak almost overlapping the peak of pure bidistilled water, which reflected the melting of the ice derived from bulk water, was present in (L/M)Ho60, (L/M)Fo60, (L/M)Ho80, and (L/M)Fo80). Regarding BD-loaded systems, it

Table 4 DSC Thermodynamic Parameters (ie, Melting Temperature and Melting Enthalpy) of the First Heating Cycle of Unloaded and BD-Loaded LCCs

	T_{m1} (°C)		T_{m2} (°C)		ΔH_{m1} (J/g)		ΔH_{m2} (J/g)	
	unloaded	BD-Loaded	Unloaded	BD-Loaded	Unloaded	BD-Loaded	Unloaded	BD-Loaded
(L/T)Ho30	-36.9	-37.1	-10.8	-5.2	-1.7	-4.0	-20.6	-38.6
(L/T)Fo30	-35.7	-35.6	-12.1	-6.4	-4.5	-4.7	-23.5	-32.5
(L/T)Ho50	-35.9	-35.8	-2.4	-2.7	-1.4	-1.8	-77.5	-88.2
(L/T)Fo50	-34.3	-34.2	-2.9	-2.0	-2.2	-2.3	-68.9	-93.1
(L/M)Ho60	-	-	-0.9	-1.2	-	-	-166.9	-157.8
(L/M)Fo60	-	-	-0.9	-1.1	-	-	-175.3	-182.7
(L/M)Ho80	-	-	-0.7	-0.8	-	-	-221.9	-220.7
(L/M)Fo80	-	-	-0.4	-0.8	-	-	-178.8	-228.2

was again confirmed that incorporation of the drug into the LCCs, where BD is predominately located in the lamellae, weakens the interactions between the surfactant and water molecules.

Regarding the melting curves of the second heating cycle of individual components ([Supplementary Figure S1D](#)), it is important to point out two endothermic peaks belonging to melting of bidistilled water ice ($T_m = -0.2\text{ }^\circ\text{C}$; $\Delta H_m = -293.4\text{ J/g}$) and evaporation of bidistilled water ($T_m = 54.4\text{ }^\circ\text{C}$; $\Delta H_m = -1578.9\text{ J/g}$) as well as one endothermic peak belonging to melting of BD ($T_m = 177.6\text{ }^\circ\text{C}$; $\Delta H_m = -154.3\text{ J/g}$). Namely, the process of melting and evaporation of bidistilled water from unloaded ([Supplementary Figure S1E](#)) and BD-loaded ([Supplementary Figure S1F](#)) LCCs can be recognized on the melting curves of the second heating cycle. Furthermore, what is even more significant is the absence of the BD melting peak in all the melting curves of BD-loaded LCCs. This led us to conclude that the drug was dissolved and uniformly distributed throughout the LCCs in its molecular state.⁵¹

Rheological Analysis

In the development phase of a drug delivery system for dermal administration, rheological analysis is particularly important as it reflects the structural characteristics that are important for its practical use. While rotational measurements address the flow behavior of a system under applied stress, referring to the structural changes upon dermal application, an insight into the viscoelastic properties of a system corresponding to its network structure is provided by oscillatory shear frequency sweep measurements.

The viscosity flow curves of all unloaded and BD-loaded LCCs recorded at 25 °C, 32 °C, and 37 °C initially decreased with increasing shear rate until they reached a constant value at high shear rates. This implies favorable shear-thinning behavior typical of non-Newtonian pseudoplastic systems. When such systems are applied to the skin, the molecules align along the flow and the viscosity decreases, which provides better spreadability on the skin surface. Subsequently, the initial viscosity is regained and thus the formulation remains at the site of action for a prolonged time.⁵² For the purpose of comparison, the viscosities of unloaded and BD-loaded LCCs determined at the lowest shear rate (1 s^{-1}) at all tested temperatures are presented in [Table 5](#). Among the unloaded LCCs, the highest viscosities at room temperature were observed for (L/T)Ho30 and (L/T)Fo30. This is consistent with the DSC analysis indicating the strongest interactions between the surfactant and water molecules in these LCCs. Namely, high viscosity is inevitably associated with strong molecular interactions within the system. Here, it is important to note that higher viscosity results in optimal consistency, enabling closer contact with the skin, which is a prerequisite for a dermal drug delivery system. In contrast, (L/T)Ho50 and (L/T)Fo50 exhibited considerably lower viscosities. These results point to an inverse correlation between the viscosity and water content of LCCs containing lecithin/Tween 80. Notably, the same relationship was also observed for LCCs containing lecithin/Montanov 68; however, the differences between the viscosities of (L/M)Ho60 and (L/M)Fo60 and (L/M)Ho80 and (L/M)Fo80 were less pronounced. The obtained data demonstrate a complex interplay between the surfactant type and water content, influencing the viscosities of all studied LCCs. Interestingly, the viscosities of the LCCs with different lipid phases (ie, hempseed and flaxseed oil) were of no significance. Considering the influence of BD incorporation, changes in viscosity were observed only in some of the studied LCCs. These results are consistent with the DSC analysis, as slightly lower viscosities

Table 5 Viscosities (Mean \pm SD ($n = 2$)) of Unloaded and BD-Loaded LCCs Determined at 25 °C, 32 °C, and 37 °C

	η (Pa s) 25 °C		η (Pa s) 32 °C		η (Pa s) 37 °C	
	Unloaded	BD-Loaded	Unloaded	BD-Loaded	Unloaded	BD-Loaded
(L/T)Ho30	282.5 \pm 3.5	227.5 \pm 4.9	226.5 \pm 2.9	195.5 \pm 4.9	212.5 \pm 3.5	175.0 \pm 4.2
(L/T)Fo30	291.5 \pm 4.5	208.5 \pm 5.9	202.5 \pm 2.1	191.5 \pm 7.8	194.5 \pm 3.5	180.0 \pm 0.7
(L/T)Ho50	19.7 \pm 0.1	15.7 \pm 0.2	15.4 \pm 0.9	14.9 \pm 0.4	11.8 \pm 0.1	13.9 \pm 0.3
(L/T)Fo50	18.9 \pm 0.2	15.4 \pm 0.1	17.7 \pm 1.3	14.2 \pm 0.2	15.1 \pm 0.5	13.3 \pm 0.5
(L/M)Ho60	40.2 \pm 1.1	39.7 \pm 0.6	34.2 \pm 0.1	27.7 \pm 0.1	24.2 \pm 0.8	19.8 \pm 0.9
(L/M)Fo60	41.3 \pm 1.3	40.3 \pm 1.9	30.5 \pm 0.4	26.1 \pm 0.4	26.7 \pm 0.9	23.9 \pm 1.1
(L/M)Ho80	13.6 \pm 0.8	13.9 \pm 0.1	8.9 \pm 0.2	7.9 \pm 0.3	6.9 \pm 0.1	7.7 \pm 0.3
(L/M)Fo80	15.6 \pm 0.2	14.4 \pm 0.4	11.4 \pm 0.1	9.1 \pm 0.1	10.1 \pm 0.1	8.1 \pm 0.1

after incorporation of BD were found solely for LCCs containing lecithin/Tween 80. This can be attributed to the partitioning of lipophilic BD into the nonpolar bilayers of these LCCs, which causes weaker interactions between the surfactant and water molecules. With regard to LCCs containing lecithin/Montanov 68, BD is presumably incorporated into the oil droplets evenly distributed within the lamellae and thus does not affect the surfactant–water interactions. Therefore, its influence on the viscosity of the LCCs was negligible. When looking at the viscosities of unloaded and BD-loaded LCCs at different tested temperatures, the viscosity decreased with increasing temperature. This is in line with our expectations, as the surfactant molecules are more loosely bound at higher temperatures, resulting in lower viscosity.

Next, rheological parameters such as storage (G') and loss (G'') moduli and complex viscosity (η^*) as a function of angular frequency were determined at 25 °C within the scope of the oscillatory measurements (Figure 5). The G'

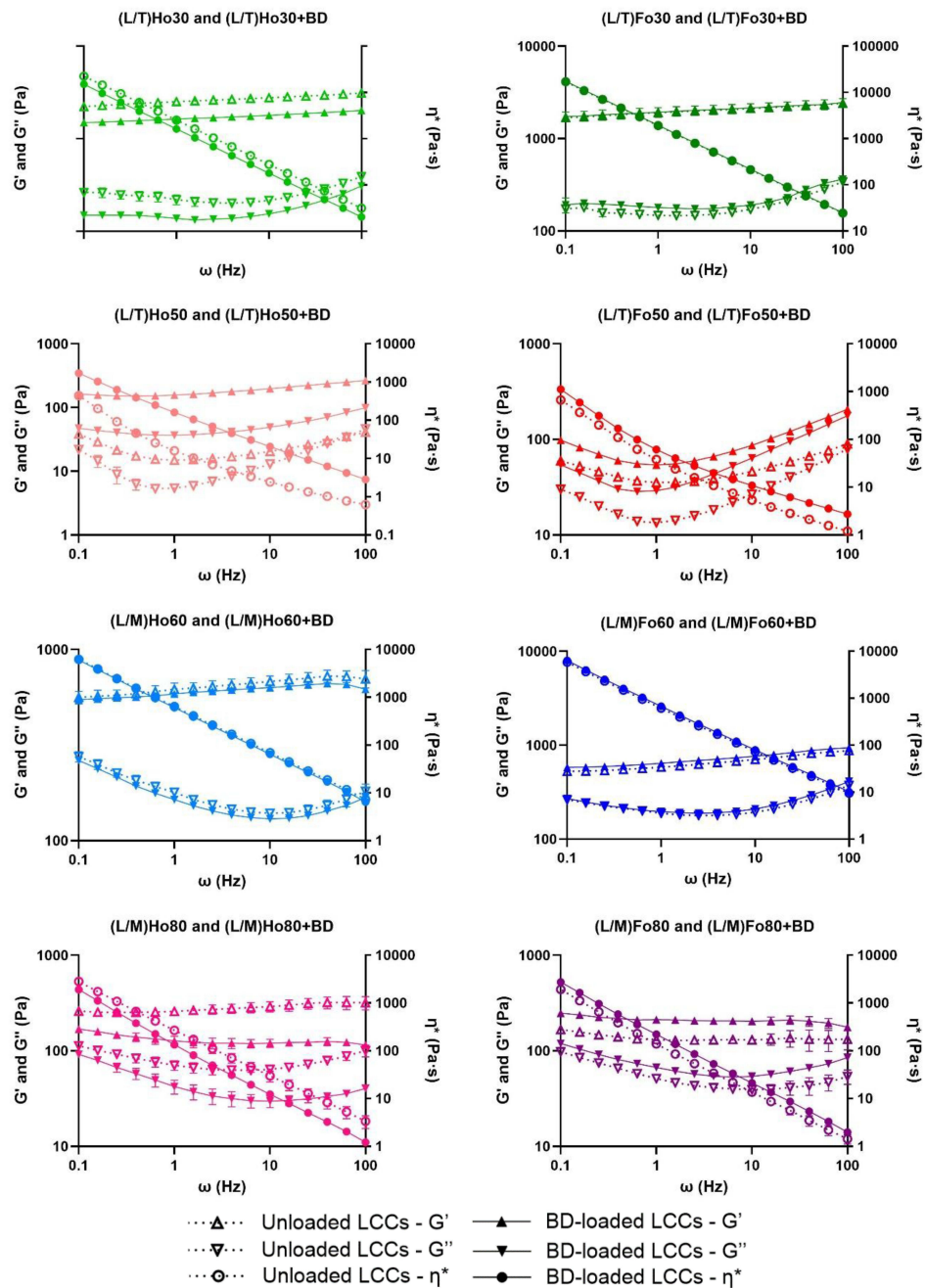


Figure 5 Storage modulus (G'), loss modulus (G''), and complex viscosity (η^*) as a function of angular frequency (ω) at a stress of 0.1% determined for unloaded and BD-loaded LCCs at 25 °C. Data are expressed as mean \pm SD ($n = 2$).

modulus reflects elastic properties, and its high values indicate high structural organization of a system, whereas high values of the G'' modulus imply viscous properties and fluid-like behavior of a system. Based on the predominant modulus, the system is classified as elastic or viscous. All unloaded LCCs exhibited higher values of G' compared to G'' , indicating more prominent elastic properties. Notably, significantly higher values of G' compared to G'' were observed for (L/T)Ho30 and (L/T)Fo30, indicating strong bilayer interactions, which is consistent with the SAXS, DSC, and rotational measurements. For all studied LCCs, both moduli were nearly independent of the angular frequency over the entire region, whereas the complex viscosity decreased rapidly with increasing frequency. Notably, this rheological behavior is characteristic of lamellar LCCs and other gel-like systems.⁵³ As for the incorporation of BD, minor changes can be observed in the values of G' and G'' moduli, but it should be emphasized that the ratios between them have been preserved, which shows that the rheological properties of the studied LCCs are comparable even after the incorporation of the drug.

Regarding the influence of elevated temperatures (ie, 32 °C and 37 °C) on the structural characteristics of unloaded and BD-loaded LCCs ([Supplementary Figure S2](#)), the results of the oscillatory tests were consistent with the findings of the rotational measurements.

Chemical Stability Study

Further consideration in the development of drug delivery systems is the evaluation of the chemical stability of the incorporated drug, as sufficient stability is crucial for the formulation of suitable finished products. BD-loaded LCCs (0.64 mg/g) were subjected to accelerated stability testing (ie, temperature of 40 ± 2 °C and relative humidity of $75 \pm 5\%$). In addition, the reference medicine comprising the same concentration of BD as BD-loaded LCCs was assessed under the same conditions for comparative purposes.

The obtained results regarding the chemical stability of the incorporated BD ([Figure 6](#)) revealed prominent differences among the studied LCCs. More specifically, (L/T)Ho30 and (L/T)Fo30 were found to be the most suitable delivery systems for BD in terms of its chemical stability. For the first one, 80.6% and for the latter 79.9% of the initial BD content was detected at the end of the stability testing, which was superior to other BD-loaded LCCs and comparable to the reference medicine (82.5%). (L/T)Ho30 and (L/T)Fo30 supremacy can be attributed to the lowest content of hydrophilic phase in these systems as it has been shown that hydrolysis of BD is triggered by elevated temperatures leading to degradation of BD. Namely, the study by Puschmann et al⁵⁴ showed that the chemical stability of BD is primarily influenced by its partitioning into the aqueous phase as degradation is typically facilitated in aqueous environment. In keeping with this, the final BD content of the other studied LCCs also decreased with increasing water content. The second highest chemical stability of the incorporated BD among the studied LCCs was observed for (L/T)Ho50 and (L/T)Fo50 with 67.5 and 69.4% final content of BD, respectively. In accordance with our

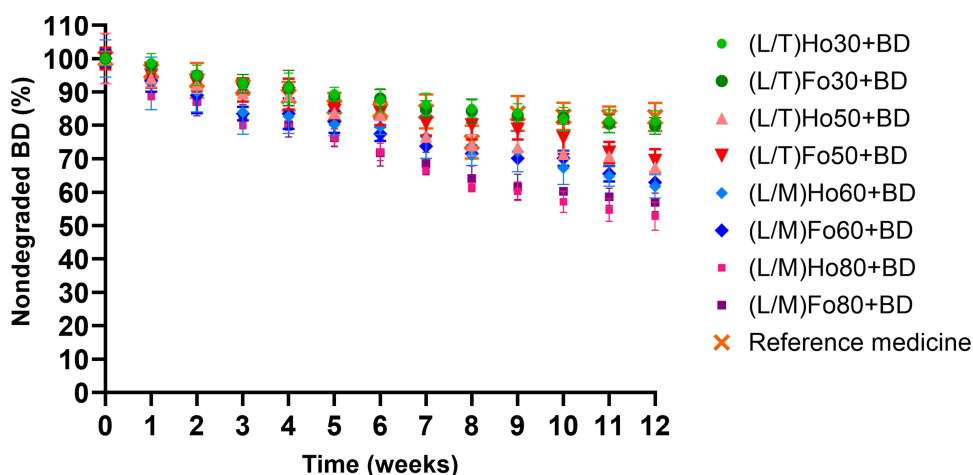


Figure 6 Content of nondegraded BD in BD-loaded LCCs and the reference medicine determined in the accelerated chemical stability study. Data are expressed as mean \pm SD (n = 3).

Table 6 First Order Degradation Kinetics of BD in BD-Loaded LCCs

	k (week ⁻¹)	R^2
(L/T)Ho30+BD	0.0028	0.946
(L/T)Fo30+BD	0.0029	0.977
(L/T)Ho50+BD	0.0038	0.978
(L/T)Fo50+BD	0.0035	0.968
(L/M)Ho60+BD	0.0057	0.969
(L/M)Fo60+BD	0.0051	0.968
(L/M)Ho80+BD	0.0080	0.983
(L/M)Fo80+BD	0.0072	0.988

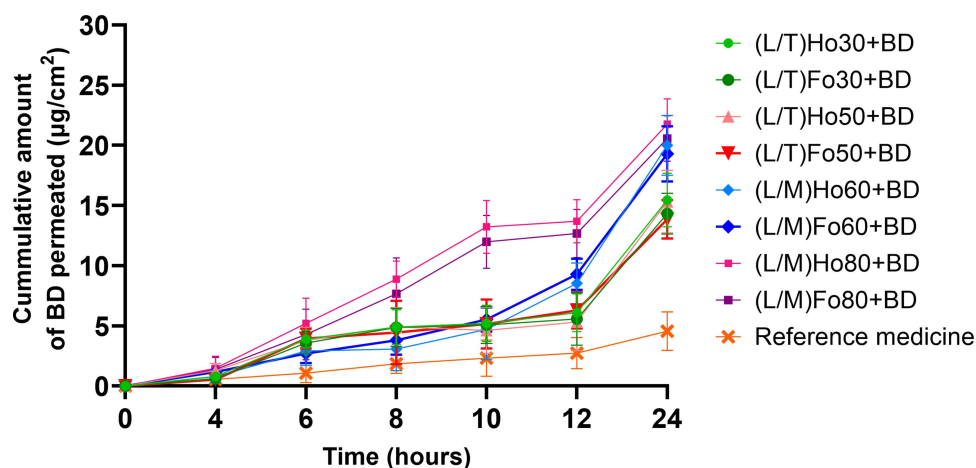
expectations due to the similar water content, these two systems were promptly followed by (L/M)Ho60 and (L/M)Fo60 with the remaining content of BD being 61.7 and 68.9%, respectively. As regards (L/M)Ho80 and (L/M)Fo80, consisting of the highest water content, they exhibited moderately low chemical stability of the incorporated drug, with a final BD content of being 52.8 and 59.6%, respectively. Further, the obtained results were also kinetically evaluated by determining the best model to describe BD degradation kinetics. Therefore, the zero- and first-order models were tested. The decrease in BD concentration followed first-order kinetics in all BD-loaded LCCs as well as in the reference medicine ($R^2 > 0.99$, Table 6).

In conclusion, we found that water, depending on its content, has a decisive influence on the chemical stability of BD incorporated into the studied LCCs. Moreover, what seems to be of major importance, (L/T)Ho30 and (L/T)Fo30 provided superior chemical stability of incorporated BD compared to the other studied LCCs. In addition, it was also proven that chemical stability of BD in these two formulations is comparable with the reference medicine.

In vitro Permeation Testing

In the next stage of our work, in vitro permeation of BD from BD-loaded LCCs (0.64 mg/g) was studied and compared with the reference medicine comprising the same concentration of BD. In vitro permeation experiments were performed using Strat-M[®], a multilayered artificial membrane system designed to mimic human skin.⁵⁵ It is composed of a tight top layer resembling *stratum corneum*, two polyether sulfone layers resembling the dermis, and a diffusive bottom layer of polyolefin resembling subcutaneous tissue. The key attributes of Strat-M[®] membranes are their ease of use, reduced safety constraints, and low batch-to-batch variability, thus providing more consistent data of *the vitro* permeation studies compared to the animal models.⁵⁶

The obtained permeation profiles of BD are shown in Figure 7. Among the studied LCCs, the highest total amount (permeated BD after 24 hours) was observed for (L/M)Ho80 (21.8 mg/cm²) and (L/M)Fo80 (20.6 mg/cm²), promptly

**Figure 7** Permeation profiles of BD from BD-loaded LCCs and the reference medicine obtained from the in vitro permeation testing. Data are expressed as mean \pm SD (n = 6).

followed by (L/M)Ho60 (20.0 mg/cm²) and (L/M)Fo60 (19.3 mg/cm²). It can be observed that BD permeation was faster from the first two LCCs compared to the latter two LCCs; however, the amount of BD permeated at the last time point was comparable for all of them. Further, moderately lower permeability was determined for (L/T)Ho50 (15.3 mg/cm²) and (L/T)Fo50 (13.9 mg/cm²) as well as (L/T)Ho30 (15.5 mg/cm²) and (L/T)Fo30 (14.3 mg/cm²). Interestingly, for these LCCs, the permeation rates were comparable.

Although all the studied LCCs differed considerably in viscosity, the obtained results supported by PLM, SAXS, and DSC analyses demonstrated that here the microstructure is the key factor influencing BD permeation. Namely, the highest total amount of permeated BD was observed for LCCs containing lecithin/Montanov 68, where BD was predominately incorporated into the oil droplets evenly distributed within the lamellae. In contrast, permeation from LCCs containing lecithin/Tween 80, where BD was localized within tightly packed lamellae, was slower. It can be implied that oil droplets facilitate the progressive diffusion of BD, while stacked bilayers of lamellae rather retard the process. This observation is also in line with the study by Gonzalez-Paredes et al.⁵⁷ The purpose of their research was to evaluate archaeal and liposomal dispersions for topical delivery of BD in terms of permeation and rheological characteristics. They found that the bilayer fluidity significantly affects penetration and accumulation in the skin strata, especially in epidermis. Nevertheless, it is important to note that all the studied LCCs showed notably improved permeation of BD compared to the reference medicine (4.6 mg/cm²), while the diffusion process was sufficiently long to avoid frequent administration. Optimizing the level of drug permeation is pivotal in achieving therapeutic efficacy while potentially facilitating dose reduction to minimize the associated adverse effects. At the same time, in the treatment of chronic diseases, such as AD, it is imperative to prolong the drug's diffusion profile sufficiently to reduce the frequency of administration, thereby enhancing patient adherence and treatment outcomes. Thus, the results confirm the potential of the studied LCCs as efficient dermal drug delivery systems for BD.

In vitro Safety Assessment

Encouraged by the promising results obtained so far, we next assessed the in vitro safety of the studied LCCs on a human keratinocyte cell line. For the purpose of comparison, the reference medicine was tested as well. Biological acceptability was evaluated using a commonly used cell proliferation assay, which provides information on changes in metabolic activity indicative of early cell damage.⁵⁸ Based on the obtained results, two most prospective LCCs and the reference medicine were selected for further evaluation. Inverted phase-contrast microscopy was employed for visual inspection of cell morphology following exposure to the samples. In addition, the assessment was upgraded using Raman microspectroscopy, capable of detecting molecular vibrations that reflect the structures and molecular characterization with no labeling. Hence, this method represents an excellent approach for investigating the cell integrity at the molecular level.⁵⁹

Cell Proliferation Assay

Cell proliferation was assessed by MTS metabolism following long term (24 hours) exposure to individual components, unloaded and BD-loaded LCCs, and the reference medicine as well. The systems were tested in a broad concentration range (0.5, 2.5, 5.0, and 10 mg/mL), revealing prominent differences in keratinocyte proliferation (Figure 8). The individual components were tested at discriminatory concentrations determined for each of the studied LCCs, taking into consideration also the content of each component in the system.

With regard to unloaded LCCs, the results clearly showed that cell proliferation was inevitably related to the concentration and composition of each system. At the lowest concentration tested, ie, 0.5 mg/mL, low cell proliferation was observed only for (L/M)Ho60 (8.1%) and (L/M)Fo60 (22.9%), while the proliferation of the other studied LCCs remained high ($\geq 80.0\%$). With increasing concentration tested, ie, 2.5 mg/mL, an evident decrease in cell proliferation was detected for (L/M)Ho80 (7.2%) and (L/M)Fo80 (2.4%). The low proliferation observed for LCCs containing lecithin/Montanov 68 can be attributed to Montanov 68. Namely, the assessment of individual components showed low proliferation after exposure to Montanov 68 ($\leq 21.5\%$), while proliferation observed for lecithin was high ($\geq 97.5\%$). Thus, the cytotoxic effect of (L/M)Ho80 and (L/M)Ho80 appeared at a higher concentration tested compared to (L/M)Ho60 and (L/M)Fo60 due to the fact that the latter consisted of a lower water content and a higher surfactant-lipid mixture content. At the next concentration tested, ie, 5.0 mg/mL, some initial differences in cell proliferation were

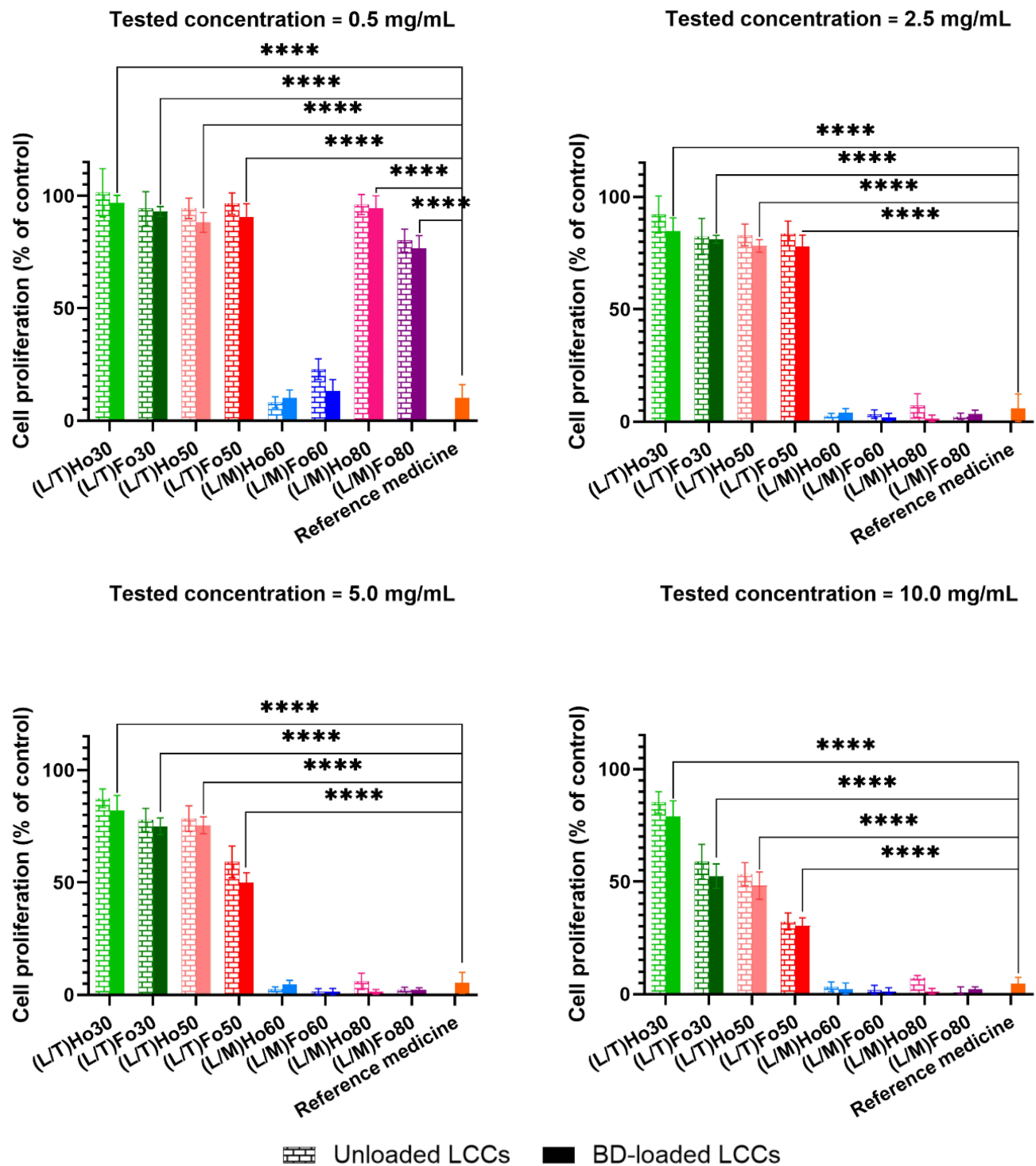


Figure 8 Keratinocyte proliferation after 24-hour exposure to unloaded LCCs, BD-loaded LCCs and the reference medicine at different tested concentrations. The results are presented relative to the proliferation of untreated control cells. Data are expressed as mean \pm SD ($n = 6$). Statistically significant differences: **** ($p < 0.0001$).

observed for LCCs containing lecithin/Tween 80 with the results ranging from 87.4% to 59.1%. However, the difference between them became more pronounced at the highest concentration tested, ie, 10.0 mg/mL, which otherwise represents a very high tested concentration for the cell proliferation assessment of colloidal drug delivery systems. It is interesting that the observations for LCCs containing lecithin/Tween 80 were opposite to the findings obtained for LCCs containing lecithin/Montanov 68. Namely, in case of lecithin/Tween 80 LCCs, higher cell proliferation was noted for systems

containing lower water content and a higher surfactant-lipid mixture content. More specifically, the cell proliferation found for (L/T)Ho30 (85.2%) stands out strongly by being much higher than for the other LCCs. The others were ranked as follows: (L/T)Fo30 (58.8%), (L/T)Ho50 (55.3%), and (L/T)Fo50 (32.3%). As here LCCs with a higher surfactant-lipid mixture content showed less cytotoxicity, and considering the cell proliferation determined after exposure to Tween 80 ($\geq 37.6\%$) and lecithin ($\geq 78.1\%$) alone, it appears that the hempseed oil supported keratinocyte proliferation to some extent.

Next, BD-loaded LCCs and the reference medicine were studied. Consistent with our expectations, cell proliferation after exposure to BD-loaded LCCs followed the same trend as that observed in the case of unloaded LCCs. However, it should be noted that, following exposure to all BD-loaded LCCs at all concentrations tested, cell proliferation was reduced by approximately 5%. This phenomenon correlates with the assessment of cell proliferation after addition of BD alone (92.03–95.5%, depending on the tested concentration) and can be attributed to the mechanism of action of BD.²⁷ In keeping with this, in the study by Guichard et al,⁶⁰ they compared the antiproliferative effect of six topical corticosteroids, including BD, on a model of hyperproliferative keratinocytes HaCaT. All topical corticosteroids reduced cell growth in a dose-dependent manner. To note, BD was found to be the most antiproliferative compound among all the tested, which supports our results as well. Further, for comparative purposes, the reference medicine was tested as well, and obtained results surprisingly showed very low cell proliferation at all tested concentrations, ie, $\leq 10.1\%$. It should be emphasized that cell proliferation was notably lower than that of all LCCs containing lecithin/Tween 80 at all tested concentrations, pointing to significant biocompatibility of these LCCs ($p < 0.0001$).

Overall, in this study, lecithin and Tween 80 were evinced as a highly biocompatible combination of surfactants, and hempseed oil was proven to be an exceptionally beneficial plant oil in terms of superior keratinocyte proliferation and biocompatibility, respectively. Accordingly, (L/T)Ho30 exhibited extraordinary cell proliferation compared to the other studied LCCs as well as the reference medicine and was thus confirmed as a highly skin-compliant BD dermal delivery system for potential treatment of AD.

Inverted Phase-Contrast Microscopy

Figure 9 displays photomicrographs from the inverted phase-contrast microscope showing the keratinocytes' morphology in culture following a 24-hour exposure to the selected LCCs, namely (L/T)Ho30 and (L/T)Fo30, as well as the reference

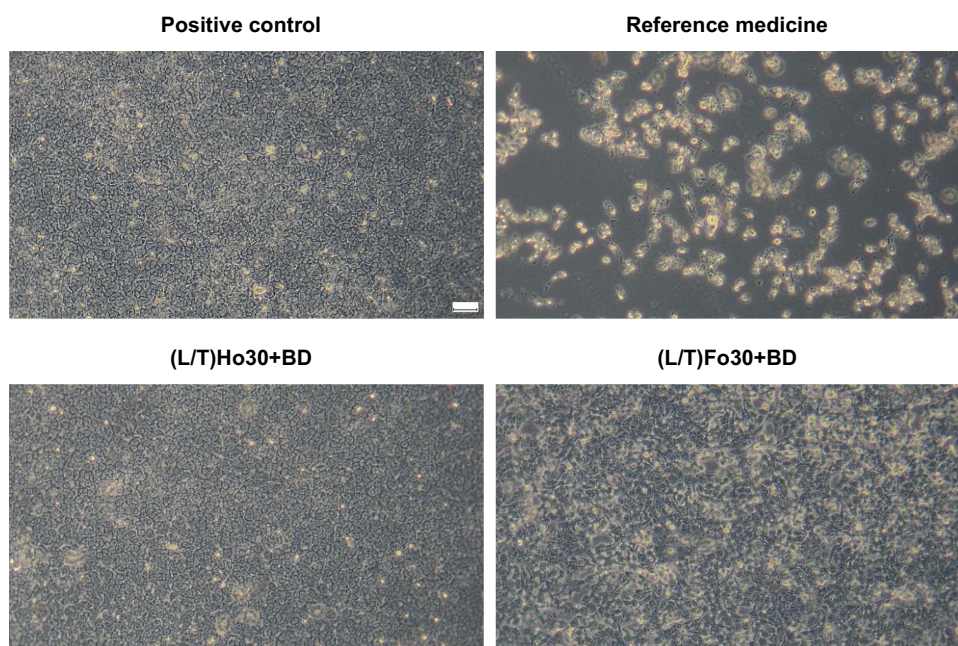


Figure 9 Morphology of keratinocytes assessed by inverted phase-contrast microscopy after 24-hour exposure to (L/T)Ho30, (L/T)Fo30, and the reference medicine, at a concentration of 5.0 mg/mL compared to the cells of the positive control. The magnification used was 20 ×. The scale bar represents 50 μm.

medicine at a concentration of 5.0 mg/mL mimicking closely the expected exposure following skin administration.⁶¹ In addition, the cells of the positive control are also presented. The observed alterations of the cell morphology in cell culture were consistent with the results of the cell proliferation assay. Namely, after exposure to (L/T)Ho30 or (L/T)Fo30, keratinocytes resembled the control cells in number and had a good surface distribution. Notably, cell culture treated with (L/T)Ho30 exhibited even denser overgrowth, and the corresponding intercellular connections were very similar to those of the positive control cells. Some minor morphological alterations concerning cell shape and the number of intercellular connections were detected in cell culture treated with (L/T)Fo30. In contrast, treatment with the reference medicine resulted in notable morphological changes, including elongated cell shapes, fewer interconnections between cells, a reduced cell number, and cell detachment from the surface.

Raman Microspectroscopy

The assessment was further upgraded using Raman microspectroscopy, which can provide a biomolecular fingerprint at the single cell level (Figure 10A). The distinct peaks in the spectrum reveal Raman scattering from various vibrational modes of the cell molecules. These data provide valuable insights into how cellular integrity is affected by various influences, whereby, in the context of developing drug delivery systems, we are particularly interested in understanding the influence of various materials used in their design.⁶² The spectral features of keratinocytes after a 24-hour exposure to the selected LCCs, namely (L/T)Ho30 and (L/T)Fo30, as well as the reference medicine at a concentration of 5.0 mg/mL, closely mimicking the expected exposure following skin administration,⁶¹ showed prominent molecular-level differences among them. For comparison purposes, spectral analysis of the positive control was also performed.

When looking at all the obtained spectra, the spectral region (680–1044 cm^{-1}) assigned to amino acids and the spectral band at 2931 cm^{-1} related to the protein state were the most noticeable.^{63,64} Regarding the latter, a significant shift to higher wavenumbers of the symmetric CH₃ stretching band, in comparison to the positive control, was observed after cellular treatment with the reference medicine, which can be attributed to the unfolding of proteins.⁶³ In addition, relatively similar observation was also found for (L/T)Fo30. In contrast, only a slight shift to higher wavenumbers at 2931 cm^{-1} was observed in case of (L/T)Ho30, indicating a preserved structure of keratinocyte proteins. In addition,

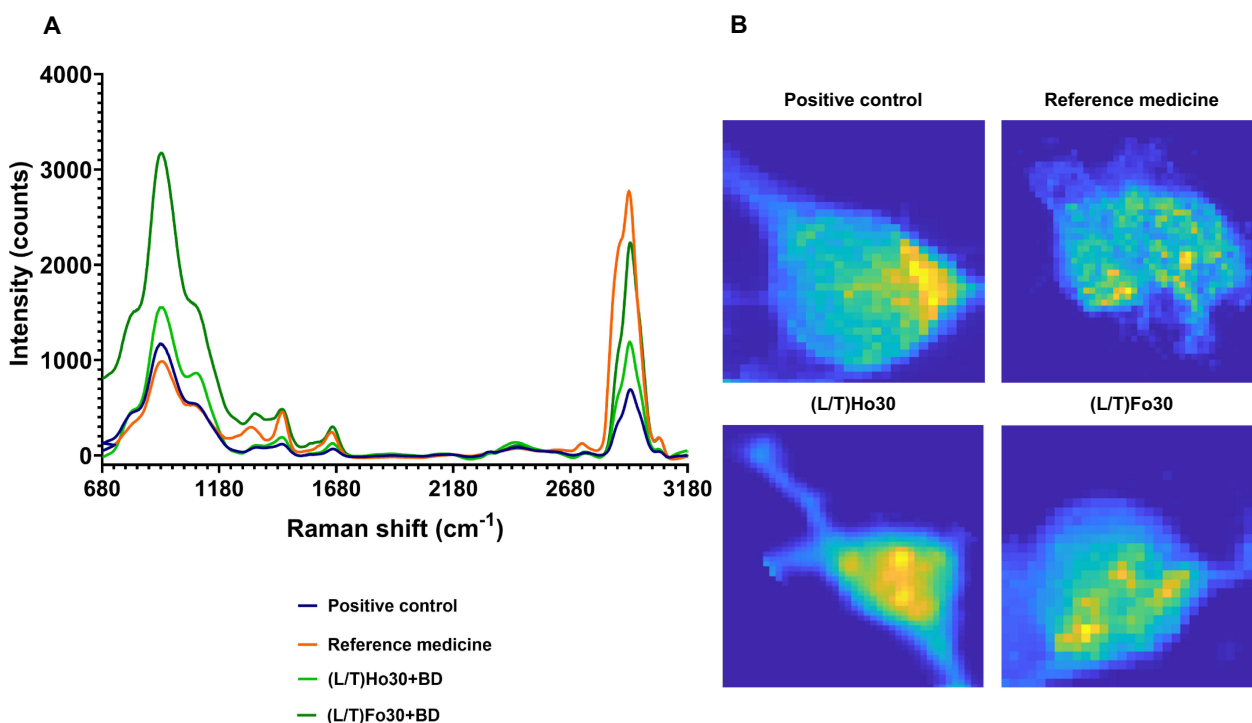


Figure 10 (A) Raman spectra and (B) hyperspectral Raman images of keratinocytes after 24-hour exposure to (L/T)Ho30, (L/T)Fo30, and the reference medicine, at a concentration of 5.0 mg/mL compared to the cells of the positive control.

alterations in the secondary structure of proteins in cells treated with the reference medicine or (L/T)Fo30 were also noted by an increase in the α -helix sub-band within the amide I band at 1658 cm^{-1} ,⁶⁵ while for (L/T)Ho30 the increase was again negligible. These results are in good agreement with the findings obtained from cell proliferation assay as well as inverted phase-contrast microscopy. Namely, cell proliferation, indirectly indicating the number of viable cells with preserved biomolecular structure, was very low after treatment with the reference medicine (5.3%), higher after treatment with (L/T)Fo30 (75.0%), and the highest after treatment with (L/T)Ho30 (82.1%), all at a tested concentration of 5.0 mg/mL. In addition, the direct visualization of the morphological characteristics following treatment with these samples supported the observed findings. Namely, treatment with the reference medicine resulted in notable morphological changes, while (L/T)Fo30 and (L/T)Ho30 exhibited subtle alterations, with (L/T)Ho30 demonstrating even denser overgrowth and intercellular connections of treated cells being almost identical to the positive control cells.

Next, interesting observations were made regarding the amino acid-related bands of tryptophan (760 cm^{-1} (ring breathing)), tyrosine (855 cm^{-1} (ring breathing) and 1044 cm^{-1}), and proline (855 cm^{-1}). As to cellular treatment with the reference medicine, a decrease in the bands related to amino acids was observed, indicating potentially vast cell damage. In contrast, a distinctive band increase in this region was observed after the cellular treatment with (L/T)Fo30. It appears that protein unfolding here contributed to the increase in amino acids present. Further, in accordance with our expectations, only a small increase in comparison with the positive control was observed for the amino acid band belonging to the cell treated with (L/T)Ho30.

Concordant with the spectral analysis, spectral imaging showing the lipid-to-protein ratio ($2820\text{--}2890\text{ cm}^{-1}$)/($2900\text{--}2970\text{ cm}^{-1}$) was also performed. According to the literature,^{63,66} the signal intensity at 2851 cm^{-1} corresponds to the region surrounding the nucleus and is specifically associated with lipids in the nuclear zone, whereas the signal intensity at 2931 cm^{-1} is linked to the state of the proteins. As shown in Figure 10B, the nucleus remained clearly identifiable in both the positive control and after the cellular treatment with (L/T)Ho30, confirming its ability to preserve keratinocytes' integrity. In contrast, after cellular treatment with (L/T)Fo30, the nucleus was difficult to identify, and core-labeling lipids were completely dispersed in the case of the reference medicine.

Gap Closure Assay

The gap closure assay is designed to in vitro simulate cell migration, providing an insight into the effectiveness of the skin healing process.⁶⁷ Figure 11 illustrates the cell migration toward the defined cell-free gap when treated with the selected LCCs, namely (L/T)Ho30 and (L/T)Fo30, and the reference medicine. The gap closure assay was performed at 0.5 mg/mL, considering the results of the cell proliferation assay, where this concentration was determined as a noncytotoxic or the most acceptable regime for LCCs and the reference medicine, respectively. In addition, the cells of the positive control are also presented.

At the first assessment time point, ie, after 12 hours cell migration was observed with both LCCs, as well as the reference medicine, with negligible differences among them. However, a comparison of all images obtained within the assays revealed some alterations in the morphology of cells treated with all three samples tested. More specifically, cells grew in clusters, which did not occur in positive control cultures. It appears that the presence of the samples induced the formation of such cell interconnections. This finding may be related to surfactants' impact on actin filaments, resulting in distinct intercellular connections as observed in our previous study, where the elasticity and morphological features of keratinocytes after exposure to LCCs were examined using atomic force microscopy.⁵⁸ The effect became even more pronounced at subsequent time points, indicating that once the cells started to connect into clusters, this unexpected type of intercellular interactions continued to develop. At the next time point of the assessment, ie, 24 hours, the mobility of cells exposed to (L/T)Ho30 was comparable to that observed in the positive control, with both exhibiting only small areas of yet unclosed gap. Slightly more cell-free space in the cell culture was observed in the culture of cells treated with (L/T)Ho30 compared to positive control. This can be attributed to the appearance of cell clusters, which contributed to slower horizontal migration of cells toward empty spaces in culture. However, the cell migration in the presence of (L/T)Ho30 at this time point was considerably higher than that observed both with (L/T)Fo30 or the reference medicine. Interestingly, even at the next time point, ie, 36 hours, the cell migration toward the cell-free area was still incomplete in the presence of (L/T)Fo30 or the reference medicine, whereas in the case of positive control and cells treated with (L/T)

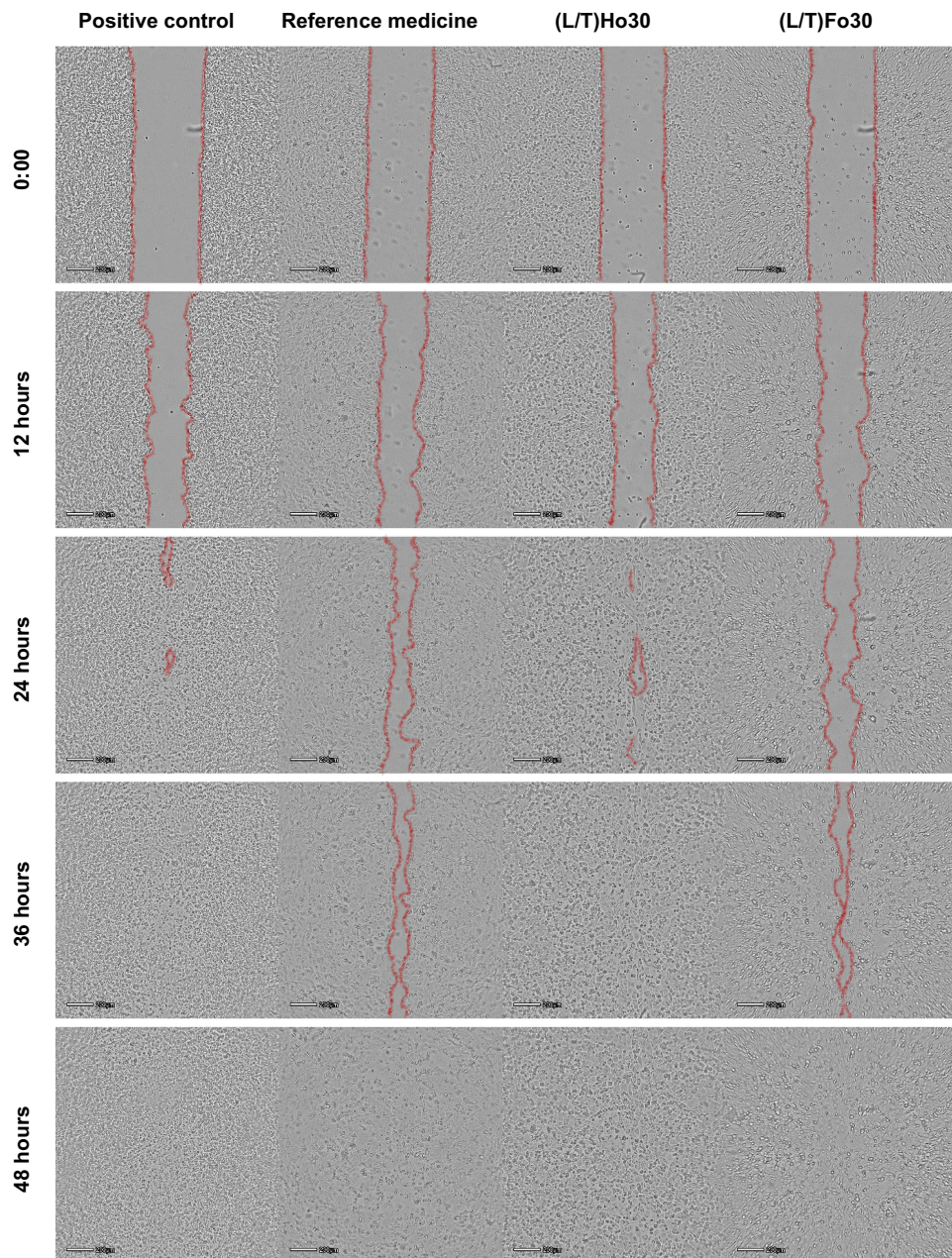


Figure 11 Representative images showing effects of (L/T)Ho30, (L/T)Fo30, and the reference medicine at a concentration of 0.5 mg/mL on keratinocytes migration toward the defined cell-free gap. In addition, the cells of the positive control are shown.

Ho30 the gaps closed completely. Only after a total of 48 hours, the cell confluence has also been reached in cultures with (L/T)Fo30 and the reference medicine.

To sum up, considering that (L/T)Ho30 and (L/T)Fo30 differed only in the type of contained plant oil, the hempseed oil promoted cell migration more efficiently in comparison to the flaxseed oil. The (L/T)Ho30 also surpassed the gap closing performance of the reference medicine. The obtained results thus indicate a potential of (L/T)Ho30 for promoting of keratinocyte migration and related skin healing effect.

Conclusions

We report here the development of innovative biomimetic lamellar LLCs based on hempseed or flaxseed oil and loaded with BD. The newly developed lamellar LCCs structurally resemble *stratum corneum* intercellular lipids, incorporate BD

drug, and consist of components that synergistically strengthen the skin barrier. Among all the LLCs studied, (L/T)Ho30 containing the highest amount of hempseed oil and lecithin/Tween 80 mixture emerged as the most promising formulation with superior functionality, performance, and biocompatibility. More specifically, PLM and SAXS confirmed the formation of lamellar mesophases with incorporated BD drug, maintaining organized microstructure at skin and physiological temperatures, while DSC indicated the presence of freezable interlamellar bound water, highlighting its skin hydration potential, and rheological analysis showed favourable viscoelastic properties for skin administration. The formulation also demonstrated suitable chemical stability of incorporated BD drug and a 3-fold enhancement in BD permeation compared to the reference medicine, with a sufficiently long diffusion process to avoid frequent administration. Furthermore, a cell proliferation assay and inverted light microscopy, along with a cell biochemical spectral analysis performed by Raman microspectroscopy, confirmed the significance of (L/T)Ho30 as a highly skin-compliant drug delivery system capable of ensuring keratinocytes' integrity. In addition, the formulation outperformed the reference medicine in terms of gap-closing performance and related skin healing effect.

In summary, a novel bioinspired approach implementing a unique multi-target drug delivery strategy for AD treatment was presented here, holding great promise for improved therapeutic outcomes and patient adherence.

Abbreviations

AD, atopic dermatitis; BD, betamethasone dipropionate; CPP, critical packing parameter; DSC, differential scanning calorimetry; HPLC, high-performance liquid chromatography; ICH, International Council for Harmonization of Technical Requirements for Pharmaceuticals for Human Use; LCCs, lyotropic liquid crystals; LOD, limit of detection; LOQ, limit of quantification; PLM, polarized light microscopy; SAXS, small-angle X-ray scattering; SD, standard deviation.

Data Sharing Statement

Data will be made available on request.

Acknowledgments

The graphical abstract was created in BioRender. Vitek, M. (2024) <https://BioRender.com/130z560>.

Funding

This study was supported by the Slovenian Research and Innovation Agency (Research Core Funding No. P1-0189 and Grant L4-4564).

Disclosure

The authors report no conflicts of interest in this work.

References

1. Mezzenga R, Seddon JM, Drummond CJ, Boyd BJ, Schröder-Turk GE, Sagalowicz L. Nature-inspired design and application of lipidic lyotropic liquid crystals. *Adv Mater.* 2019;31(35):1900818. doi:10.1002/adma.201900818
2. Hag LVT, Gras SL, Conn CE, Drummond CJ. Lyotropic liquid crystal engineering moving beyond binary compositional space – ordered nanostructured amphiphile self-assembly materials by design. *Chem Soc Rev.* 2017;46(10):2705–2731. doi:10.1039/C6CS00663A
3. Chavda VP, Dyawanapelly S, Dawre S, et al. Lyotropic liquid crystalline phases: drug delivery and biomedical applications. *Int J Pharm.* 2023;647:123546. doi:10.1016/j.ijpharm.2023.123546
4. Silvestrini AVP, Caron AL, Viegas J, Praça FG, Bentley MVLB. Advances in lyotropic liquid crystal systems for skin drug delivery. *Expert Opin Drug Deliv.* 2020;17(12):1781–1805. doi:10.1080/17425247.2020.1819979
5. Kozaka S, Wakabayashi R, Kamiya N, Goto M. Lyotropic liquid crystal-based transcutaneous peptide delivery system: evaluation of skin permeability and potential for transcutaneous vaccination. *Acta Biomater.* 2022;138:273–284. doi:10.1016/j.actbio.2021.11.008
6. Rapalli VK, Waghule T, Hans N, et al. Insights of lyotropic liquid crystals in topical drug delivery for targeting various skin disorders. *J Mol Liq.* 2020;315:113771. doi:10.1016/j.molliq.2020.113771
7. Zabara A, Mezzenga R. Controlling molecular transport and sustained drug release in lipid-based liquid crystalline mesophases. *J Control Release.* 2014;188:31–43. doi:10.1016/j.jconrel.2014.05.052
8. Shoib A, Mangla B, Javed S, Sultan MH, Alqahtani SS, Shakeel F. Vicissitudes of liquid crystals for solubility enhancement of poorly soluble drugs. *J Mol Liq.* 2021;321:114924. doi:10.1016/j.molliq.2020.114924

9. Huang Y, Gui S. Factors affecting the structure of lyotropic liquid crystals and the correlation between structure and drug diffusion. *RSC Adv.* 2018;8(13):6978–6987. doi:10.1039/C7RA12008G
10. Carità AC, Resende de Azevedo J, Vinicius Buri M, et al. Stabilization of vitamin C in emulsions of liquid crystalline structures. *Int J Pharm.* 2021;592:120092. doi:10.1016/j.ijpharm.2020.120092
11. Vitek M, Gosenca Matjaž M, Roškar R, Gašperlin M, Zvonar Pobirk A. A comparative study of lipid-based drug delivery systems with different microstructure for combined dermal administration of antioxidant vitamins. *J Disper Sci Technol.* 2022;1–14. doi:10.1080/01932691.2022.2037437
12. Elnaggar YS, Talaat SM, Bahey-El-Din M, Abdallah OY. Novel lecithin-integrated liquid crystalline nanogels for enhanced cutaneous targeting of terconazole: development, in vitro and in vivo studies. *Int J Nanomed.* 2016;11:5531–5547. doi:10.2147/IJN.S117817
13. Danciu C, Berkó S, Varju G, et al. The effect of electroporation of a lyotropic liquid crystal genistein-based formulation in the recovery of murine melanoma lesions. *Int J Mol Sci.* 2015;16(7):15425–15441. doi:10.3390/ijms160715425
14. Mercier MF, Thau P, Chase J Multi-lamellar liquid crystal emulsion system. Available from: <https://patents.google.com/patent/US7754775B2/en>. Accessed February 12, 2024.
15. Iwai H, Fukasawa J, Suzuki T. A liquid crystal application in skin care cosmetics. *Int J Cosmet Sci.* 1998;20(2):87–102. doi:10.1046/j.1467-2494.1998.171741.x
16. Li Z, Zhao X, Wang Z. Study on the formation and rheological properties of sucrose stearate lamellar liquid crystals. *J Disper Sci Technol.* 2017;38(1):152–158. doi:10.1080/01932691.2016.1147360
17. Shah V, Bharatiya B, Gawali S, et al. Thermoresponsive liquid crystalline formulation of exemestane: design and structural characterization. *Colloids Surf B Biointerfaces.* 2021;202:111683. doi:10.1016/j.colsurfb.2021.111683
18. Langan SM, Irvine AD, Weidinger S. Atopic dermatitis. *Lancet.* 2020;396(10247):345–360. doi:10.1016/S0140-6736(20)31286-1
19. Weidinger S, Beck LA, Bieber T, Kabashima K, Irvine AD. Atopic dermatitis. *Nat Rev Dis Primers.* 2018;4(1):1. doi:10.1038/s41572-018-0001-z
20. Bhattacharya N, Sato WJ, Kelly A, Ganguli-Indra G, Indra AK. Epidermal lipids: key mediators of atopic dermatitis pathogenesis. *Trends Mol Med.* 2019;25(6):551–562. doi:10.1016/j.molmed.2019.04.001
21. Montero-Vilchez T, Segura-Fernández-Nogueras MV, Pérez-Rodríguez I, et al. Skin barrier function in psoriasis and atopic dermatitis: transepidermal water loss and temperature as useful tools to assess disease severity. *J Clin Med.* 2021;10(2):359. doi:10.3390/jcm10020359
22. Yang G, Seok JK, Kang HC, Cho YY, Lee HS, Lee JY. Skin barrier abnormalities and immune dysfunction in atopic dermatitis. *Int J Mol Sci.* 2020;21(8):E2867. doi:10.3390/ijms21082867
23. Bertino L, Guarneri F, Cannavò SP, Casciaro M, Pioggia G, Gangemi S. Oxidative stress and atopic dermatitis. *Antioxidants.* 2020;9(3):196. doi:10.3390/antiox9030196
24. Wollenberg A, Barbarot S, Bieber T, et al. Consensus-based European guidelines for treatment of atopic eczema (atopic dermatitis) in adults and children: part I. *J Eur Acad Dermatol Venereol.* 2018;32(5):657–682. doi:10.1111/jdv.14891
25. Wollenberg A, Barbarot S, Bieber T, et al. Consensus-based European guidelines for treatment of atopic eczema (atopic dermatitis) in adults and children: part II. *J Eur Acad Dermatol Venereol.* 2018;32(6):850–878. doi:10.1111/jdv.14888
26. Chu DK, Schneider L, Asiniwasis RN, et al. Atopic dermatitis (eczema) guidelines: 2023 American Academy of Allergy, Asthma and Immunology/ American College of Allergy, Asthma and Immunology joint task force on practice parameters GRADE- and institute of medicine-based recommendations. *Ann Allergy Asthma Immunol.* 2023;2023. doi:10.1016/j.anai.2023.11.009
27. Diaz A, Guttman-Yassky E. Topical agents for the treatment of atopic dermatitis. *Expert Rev Clin Immunol.* 2019;15(4):369–382. doi:10.1080/1744666X.2019.1564038
28. Mandlik DS, Mandlik SK. Atopic dermatitis: new insight into the etiology, pathogenesis, diagnosis and novel treatment strategies. *Immunopharm Immunot.* 2021;43(2):105–125. doi:10.1080/08923973.2021.1889583
29. Vitorović J, Joković N, Radulović N, et al. Antioxidant activity of Hemp (*Cannabis sativa* L.) seed oil in *Drosophila melanogaster* Larvae under non-stress and H₂O₂-induced oxidative stress conditions. *Antioxidants.* 2021;10(6):830. doi:10.3390/antiox10060830
30. Gutiérrez S, Svahn SL, Johansson ME. Effects of omega-3 fatty acids on immune cells. *Int J Mol Sci.* 2019;20(20):5028. doi:10.3390/ijms20205028
31. Yang J, Min S, Hong S. Therapeutic effects of fermented flax seed oil on NC/Nga mice with atopic dermatitis-like skin lesions. *Evid Based Complement Alternat Med.* 2017;2017:5469125. doi:10.1155/2017/5469125
32. Sergeant S, Rahbar E, Chilton FH. Gamma-linolenic acid, Dihommo-gamma linolenic, eicosanoids and inflammatory processes. *Eur J Pharmacol.* 2016;785:77–86. doi:10.1016/j.ejphar.2016.04.020
33. Ansari R, Zarshenas MM, Dadbakhsh AH. A review on pharmacological and clinical aspects of *Linum usitatissimum* L. *Curr Drug Discov Technol.* 2019;16(2):148–158. doi:10.2174/1570163815666180521101136
34. Terescenco D, Picard C, Clemenceau F, Grisel M, Savary G. Influence of the emollient structure on the properties of cosmetic emulsion containing lamellar liquid crystals. *Colloids Surf a Physicochem.* 2018;536:10–19. doi:10.1016/j.colsurfa.2017.08.017
35. Gosenca M, Bešter-Rogač M, Gašperlin M. Lecithin based lamellar liquid crystals as a physiologically acceptable dermal delivery system for ascorbyl palmitate. *Eur J Pharm Sci.* 2013;50(1):114–122. doi:10.1016/j.ejps.2013.04.029
36. Wang X, Zhang Y, Gui S, et al. Characterization of lipid-based lyotropic liquid crystal and effects of guest molecules on its microstructure: a systematic review. *AAPS Pharm Sci Tech.* 2018;19(5):2023–2040. doi:10.1208/s12249-018-1069-1
37. Glatter O, Salentinig S. Inverting structures: from micelles via emulsions to internally self-assembled water and oil continuous nanocarriers. *Curr Opin Colloid Interface Sci.* 2020;49:82–93. doi:10.1016/j.cocis.2020.05.003
38. Kumar VV. Complementary molecular shapes and additivity of the packing parameter of lipids. *Proc Natl Acad Sci U S A.* 1991;88(2):444–448. doi:10.1073/pnas.88.2.444
39. Amani A, York P, de WH, Anwar J. Molecular dynamics simulation of a polysorbate 80 micelle in water. *Soft Matter.* 2011;7(6):2900–2908. doi:10.1039/C0SM00965B
40. Rong G, Yang J, Friberg SE, Aikens PA, Greenshields JN. Complex lamellar structure of Polyoxyethylene 20 sorbitan oleate and a fatty acid/lecithin lamellar liquid crystal. *Langmuir.* 1996;12(17):4286–4291. doi:10.1021/la960059c
41. Mkam Tsengam IK, Omarova M, Kelley EG, et al. Transformation of lipid vesicles into micelles by adding nonionic surfactants: elucidating the structural pathway and the intermediate structures. *J Phys Chem B.* 2022;126(11):2208–2216. doi:10.1021/acs.jpcc.1c09685

42. Savić S, Vuleta G, Daniels R, Müller-Goymann CC. Colloidal microstructure of binary systems and model creams stabilized with an alkylpolyglucoside non-ionic emulsifier. *Colloid Polym Sci.* 2005;283(4):439–451. doi:10.1007/s00396-004-1174-4
43. Ahmadi D, Mahmoudi N, Li P, et al. Revealing the hidden details of nanostructure in a pharmaceutical cream. *Sci Rep.* 2020;10(1):4082. doi:10.1038/s41598-020-61096-x
44. Alexandridis P, Olsson U, Lindman B. A record nine different phases (four cubic, two hexagonal, and one lamellar lyotropic liquid crystalline and two micellar solutions) in a ternary isothermal system of an amphiphilic block copolymer and selective solvents (water and oil). *Langmuir.* 1998;14(10):2627–2638. doi:10.1021/la971117c
45. Battista S, Marsicano V, Arcadi A, et al. UV properties and loading into liposomes of quinoline derivatives. *Colloids Interfaces.* 2021;5(2):28. doi:10.3390/colloids5020028
46. Rymaruk MJ, O'Brien CT, György C, et al. Small-angle X-ray scattering studies of block copolymer nano-objects: formation of ordered phases in concentrated solution during polymerization-induced self-assembly. *Angew Chem Int Ed Engl.* 2021;60(23):12955–12963. doi:10.1002/anie.202101851
47. Zhuang W, Chen X, Cai J, Zhang G, Qiu H. Characterization of lamellar phases fabricated from Brij-30/water/1-butyl-3-methylimidazolium salts ternary systems by small-angle X-ray scattering. *Colloids Surf a Physicochem.* 2008;318(1):175–183. doi:10.1016/j.colsurfa.2007.12.034
48. Bag MA, Valenzuela LM. Impact of the hydration states of polymers on their hemocompatibility for medical applications: a review. *Int J Mol Sci.* 2017;18(8):1422. doi:10.3390/ijms18081422
49. Kodama M, Kawasaki Y, Aoki H, Furukawa Y. Components and fractions for differently bound water molecules of dipalmitoylphosphatidylcholine-water system as studied by DSC and 2H-NMR spectroscopy. *Biochim Biophys Acta.* 2004;1667(1):56–66. doi:10.1016/j.bbmem.2004.08.015
50. Kodama M, Nakamura J, Miyata T, Aoki H. The behaviour of water molecules associated with structural changes in negatively charged phosphatidyl-glycerol assemblies as studied by DSC. *J Therm Anal Calorim.* 1998;51(1):91–104. doi:10.1007/BF02719013
51. Timotijević MD, Ilić T, Marković B, et al. Coupling AFM, DSC and FT-IR towards elucidation of film-forming systems transformation to dermal films: a betamethasone dipropionate case study. *Int J Mol Sci.* 2022;23(11):6013. doi:10.3390/ijms23116013
52. Fonseca-Santos B, Satake CY, Calixto GMF, dos SAM, Chorilli M. Trans-resveratrol-loaded nonionic lamellar liquid-crystalline systems: structural, rheological, mechanical, textural, and bioadhesive characterization and evaluation of in vivo anti-inflammatory activity. *Int J Nanomed.* 2017;12:6883. doi:10.2147/IJN.S138629
53. Berni MG, Lawrence CJ, Machin D. A review of the rheology of the lamellar phase in surfactant systems. *Adv Colloid Interface Sci.* 2002;98(2):217–243. doi:10.1016/s0001-8686(01)00094-x
54. Puschmann J, Herbig ME, Müller-Goymann CC. Influence of emulsifier concentration on partition behavior and chemical stability of betamethasone dipropionate in emulsion gels. *Int J Pharm.* 2019;562:105–112. doi:10.1016/j.ijpharm.2019.02.044
55. Ferrara F, Benedusi M, Cervellati F, et al. Dimethyl fumarate-loaded transthesosomes: a formulative study and preliminary ex vivo and in vivo evaluation. *Int J Mol Sci.* 2022;23(15):8756. doi:10.3390/ijms23158756
56. Milanowski B, Wosicka-Fraćkowiak H, Główska E, et al. Optimization and evaluation of the in vitro permeation parameters of topical products with non-steroidal anti-inflammatory drugs through strat-M[®] membrane. *Pharmaceutics.* 2021;13(8):1305. doi:10.3390/pharmaceutics13081305
57. González-Paredes A, Manconi M, Caddeo C, Ramos-Cormenzana A, Monteoliva-Sánchez M, Fadda AM. Archaeosomes as carriers for topical delivery of betamethasone dipropionate: in vitro skin permeation study. *J Liposome Res.* 2010;20(4):269–276. doi:10.3109/08982100903402962
58. Matjaž M G, Škarabot M, Gašperlin M, Janković B. Lamellar liquid crystals maintain keratinocytes' membrane fluidity: an AFM qualitative and quantitative study. *Int J Pharm.* 2019;572:118712. doi:10.1016/j.ijpharm.2019.118712
59. Dodo K, Fujita K, Sodeoka M. Raman spectroscopy for chemical biology research. *J Am Chem Soc.* 2022;144(43):19651–19667. doi:10.1021/jacs.2c05359
60. Guichard A, Humbert P, Tissot M, Muret P, Courderot-Masuyer C, Viennet C. Effects of topical corticosteroids on cell proliferation, cell cycle progression and apoptosis: in vitro comparison on HaCaT. *Int J Pharm.* 2015;479(2):422–429. doi:10.1016/j.ijpharm.2014.12.066
61. Im JE, Kim HY, Lee JD, Park JJ, Kang KS, Kim KB. Effect of application amounts on in vitro dermal absorption test using caffeine and testosterone. *Pharmaceutics.* 2021;13(5):641. doi:10.3390/pharmaceutics13050641
62. Liu Y, Li M, Liu H, Kang C, Yu X. Strategies and progress of Raman technologies for cellular uptake analysis of the drug delivery systems. *Int J Nanomed.* 2023;18:6883–6900. doi:10.2147/IJN.S435087
63. Bakar J, Michael-Jubeli R, Tfaïli S, Assi A, Baillet-Guffroy A, Tfaïli A. Biomolecular modifications during keratinocyte differentiation: raman spectroscopy and chromatographic techniques. *Analyst.* 2021;146(9):2965–2973. doi:10.1039/D1AN00231G
64. Franzen L, Windbergs M. Applications of Raman spectroscopy in skin research--From skin physiology and diagnosis up to risk assessment and dermal drug delivery. *Adv Drug Deliv Rev.* 2015;89:91–104. doi:10.1016/j.addr.2015.04.002
65. Choe C, Schleusener J, Lademann J, Darvin ME. Keratin-water-NMF interaction as a three layer model in the human stratum corneum using in vivo confocal Raman microscopy. *Sci Rep.* 2017;7(1):15900. doi:10.1038/s41598-017-16202-x
66. Egawa M, Tokunaga K, Hosoi J, Iwanaga S, Ozeki Y. In situ visualization of intracellular morphology of epidermal cells using stimulated Raman scattering microscopy. *J Biomed Opt.* 2016;21(8):086017. doi:10.1117/1.JBO.21.8.086017
67. Huang Y, Chen Y, Cheng G, et al. A TA/Cu²⁺ nanoparticle enhanced carboxymethyl chitosan-based hydrogel dressing with antioxidant properties and promoting wound healing. *Int J Nanomed.* 2024;19:231–245. doi:10.2147/IJN.S445844

International Journal of Nanomedicine

Dovepress

Publish your work in this journal

The International Journal of Nanomedicine is an international, peer-reviewed journal focusing on the application of nanotechnology in diagnostics, therapeutics, and drug delivery systems throughout the biomedical field. This journal is indexed on PubMed Central, MedLine, CAS, SciSearch[®], Current Contents[®]/Clinical Medicine, Journal Citation Reports/Science Edition, EMBase, Scopus and the Elsevier Bibliographic databases. The manuscript management system is completely online and includes a very quick and fair peer-review system, which is all easy to use. Visit <http://www.dovepress.com/testimonials.php> to read real quotes from published authors.

Submit your manuscript here: <https://www.dovepress.com/international-journal-of-nanomedicine-journal>